



Ross Sea paleo-ice sheet drainage and deglacial history during and since the LGM[☆]



John B. Anderson ^{a,*}, Howard Conway ^b, Philip J. Bart ^c, Alexandra E. Witus ^a, Sarah L. Greenwood ^d, Robert M. McKay ^e, Brenda L. Hall ^{f,g}, Robert P. Ackert ^h, Kathy Licht ⁱ, Martin Jakobsson ^d, John O. Stone ^b

^a Department of Earth Sciences, Rice University, 6100 Main Street, Houston, TX, USA

^b Department of Earth and Space Sciences, University of Washington, 4000 15th Avenue NE, Seattle, WA, USA

^c Department of Geology and Geophysics, Louisiana State University, Baton Rouge, LA, USA

^d Department of Geological Sciences, Stockholm University, Stockholm, Sweden

^e Antarctic Research Centre, P.O. Box 600, Victoria University of Wellington, New Zealand

^f School of Earth and Climate Sciences, University of Maine, Orono, ME, USA

^g Climate Change Institute, University of Maine, Orono, ME, USA

^h Department of Earth and Planetary Science, Harvard University, Cambridge, MA, USA

ⁱ Department of Earth Sciences, Indiana University-Purdue University Indianapolis, 723 West Michigan Street, SL118, Indianapolis, IN, USA

ARTICLE INFO

Article history:

Received 16 January 2013

Received in revised form

23 July 2013

Accepted 25 August 2013

Available online 8 October 2013

Keywords:

Ross Sea

Glacial history

LGM–post LGM

Paleodrainage

ABSTRACT

Onshore and offshore studies show that an expanded, grounded ice sheet occupied the Ross Sea Embayment during the Last Glacial Maximum (LGM). Results from studies of till provenance and the orientation of geomorphic features on the continental shelf show that more than half of the grounded ice sheet consisted of East Antarctic ice flowing through Transantarctic Mountain (TAM) outlet glaciers; the remainder came from West Antarctica. Terrestrial data indicate little or no thickening in the upper catchment regions in both West and East Antarctica during the LGM. In contrast, evidence from the mouths of the southern and central TAM outlet glaciers indicate surface elevations between 1000 m and 1100 m (above present-day sea level). Farther north along the western margin of the Ross Ice Sheet, surface elevations reached 720 m on Ross Island, and 400 m at Terra Nova Bay. Evidence from Marie Byrd Land at the eastern margin of the ice sheet indicates that the elevation near the present-day grounding line was more than 800 m asl, while at Siple Dome in the central Ross Embayment, the surface elevation was about 950 m asl. Farther north, evidence that the ice sheet was grounded on the middle and the outer continental shelf during the LGM implies that surface elevations had to be at least 100 m above the LGM sea level. The apparent low surface profile and implied low basal shear stress in the central and eastern embayment suggests that although the ice streams may have slowed during the LGM, they remained active.

Ice-sheet retreat from the western Ross Embayment during the Holocene is constrained by marine and terrestrial data. Ages from marine sediments suggest that the grounding line had retreated from its LGM outer shelf location only a few tens of kilometer to a location south of Coulman Island by ~13 ka BP. The ice sheet margin was located in the vicinity of the Drygalski Ice Tongue by ~11 ka BP, just north of Ross Island by ~7.8 ka BP, and near Hatherton Glacier by ~6.8 ka BP. Farther south, ¹⁰Be exposure ages from glacial erratics on nunataks near the mouths of Reedy, Scott and Beardmore Glaciers indicate thinning during the mid to late Holocene, but the grounding line did not reach its present position until 2 to 3 ka BP. Marine dates, which are almost exclusively Acid Insoluble Organic (AIO) dates, are consistently older than those derived from terrestrial data. However, even these ages indicate that the ice sheet experienced significant retreat after ~13 ka BP. Geomorphic features indicate that during the final stages of ice sheet retreat ice flowing through the TAM remained grounded on the shallow western margin of Ross Sea.

The timing of retreat from the central Ross Sea remains unresolved; the simplest reconstruction is to assume that the grounding line here started to retreat from the continental shelf more or less in step with the retreat from the western and eastern sectors. An alternative hypothesis, which relies on the

[☆] This is an open access article under the CC BY license (<http://creativecommons.org/licenses/by/3.0/>).

* Corresponding author.

E-mail address: johna@rice.edu (J.B. Anderson).

validity of radiocarbon ages from marine sediments, is that grounded ice had retreated from the outer continental shelf prior to the LGM. More reliable ages from marine sediments in the central Ross Embayment are needed to test and validate this hypothesis.

© 2014 The Authors. Published by Elsevier Ltd. All rights reserved.

1. Introduction

Reconstructions of past changes in thickness and extent of the Antarctic ice sheet are important for evaluating past and present sea-level change, and for validating numerical models necessary to make realistic predictions of changes under future climate and ocean conditions.

The catchment for the Ross Sea sector today includes $\sim 1.65 \times 10^6 \text{ km}^2$ from the East Antarctic Ice Sheet (EAIS), and $0.75 \times 10^6 \text{ km}^2$ from the West Antarctic Ice Sheet (WAIS) (Rignot et al., 2008) (Fig. 1). The mass balance of the Ross Sea sector has been positive ($\sim 40 \text{ Gt/yr}$ – Rignot et al., 2008) since the stagnation of Kamb Ice Stream about 180 years ago and the recent slow-down of Whillans Ice Stream (Joughin and Tulaczyk, 2002). It is not yet clear whether this apparent positive imbalance is part of century-scale fluctuations of the ice streams (Hulbe and Fahnestock, 2007), or whether it represents a reversal of the long-term Holocene retreat of the ice sheet (Conway et al., 1999; Hall et al., 2013). To help address this question, here we present a synthesis of the late Quaternary glacial history of the Ross Sea sector and provide reconstructions of LGM and post-LGM ice-sheet configurations. These reconstructions are also intended to aid in the evaluation of Antarctica's contribution to post-LGM sea-level rise, as well as to provide constraints to test the accuracy of ice sheet models.

2. LGM ice-sheet extent and thickness

Scott (1905) and David and Priestley (1914) were the first to document evidence for more extreme "Ice Age" conditions in the Ross Sea. Since then, there have been numerous investigations of the late Quaternary glacial history of the region, both onshore and offshore. Yet, there is still uncertainty regarding the extent, thickness, flow configuration, and timing of the expanded ice sheet and its deglaciation history. Here we use the term Last Glacial Maximum (LGM) as it refers to global ice-sheet expansion ~ 26.5 to 19 ka BP (Clark et al., 2009), although below we show that grounded ice remained close to its maximum extent for significantly longer than this interval in parts of the Ross Sea Embayment.

2.1. Marine geologic evidence

2.1.1. LGM extent and paleodrainage

Several hundred sediment cores have been collected in the Ross Sea, and numerous studies have focused on distinguishing between tills and glacimarine sediments, which is required for reconstructing glacial history (Kellogg et al., 1979; Anderson et al., 1980, 1983, 1992; Domack et al., 1999; Licht et al., 1999; Licht and Andrews, 2002; Mosola and Anderson, 2006). Early work mapped till distribution based on the presence of over-consolidated diamictons, but introduction of the concept of deformation till in the late 1980's (Alley et al., 1986) expanded the classification to include soft, water-saturated till deposits, which had previously been ascribed a proximal glacimarine origin. The combined results from sedimentological studies show that till and proximal glacimarine sediments are widespread on the continental shelf, indicating that grounded ice extended across most of the shelf in the past (Fig. 2).

The typical stratigraphic succession of deposits sampled in piston cores from the western Ross Sea consists of an upward progression from till to proximal glacimarine to distal glacimarine sediments that generally show increasing abundance of diatomaceous material upwards (Anderson et al., 1992; Domack et al., 1999; Licht et al., 1999; McKay et al., 2008). This succession records a progressive landward shift in the retreating grounding line across the continental shelf and eventual onset of periodic open-marine conditions. Domack et al. (1999) identified a pelletized sub-ice shelf facies deposited during the initial retreat phase of the ice-sheet grounding line, overlain by a thin mud facies lacking coarse-grained material deposited in the so-called ice shelf "null zone". McKay et al. (2008) studied cores collected 5 km upstream from the present-day ice shelf edge. They recognized three sub-ice shelf glacimarine facies: a clast-rich diamicton with low concentrations of fragmented diatoms overlain by well-sorted laminated sand that lies in sharp contact with massive mud. The well-sorted laminated sand facies is notably absent in cores from the Ross Sea continental shelf, which could have implications about the history of the ice shelf, or it may simply reflect unique oceanographic conditions in the area where the cores studied by McKay et al. (2008) were collected.

The youngest sedimentary facies in the western Ross Sea is a diatomaceous glacimarine facies, which contains minor ice rafted debris indicative of seasonally open-marine conditions (Cunningham et al., 1999; Domack et al., 1999; Licht et al., 1999;

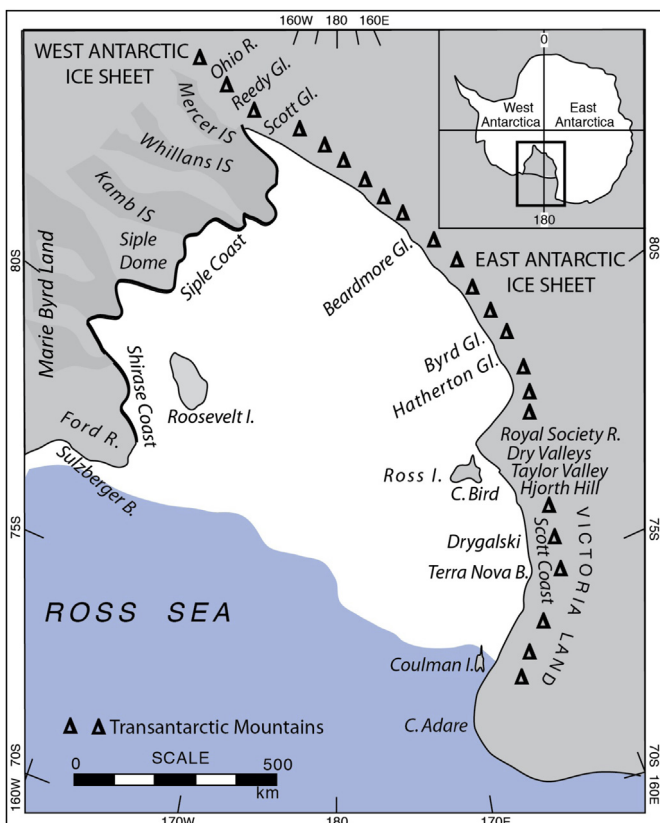


Fig. 1. Geographic map showing locations referred to in text.

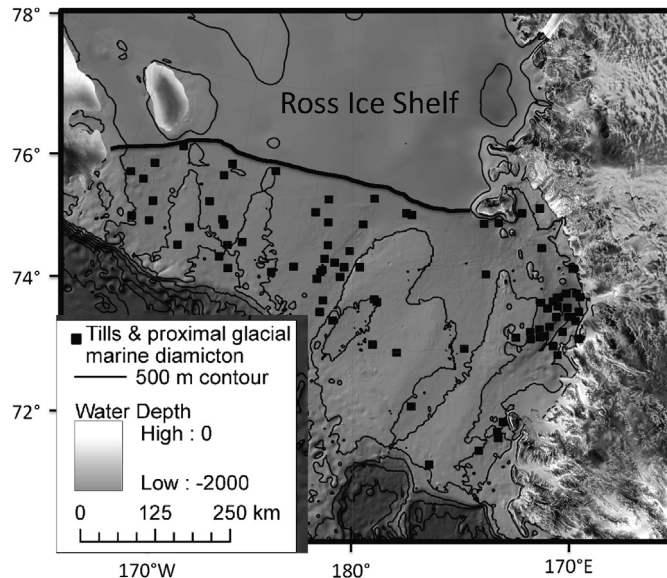


Fig. 2. Locations of sediment cores for which detailed sedimentological analyses have been conducted and diamictites have been interpreted as either till or proximal glacimarine sediments (see text for sources). Prior to the advent of multibeam swath bathymetry, these data were used to locate the grounding line of the expanded ice sheet.

(McKay et al., 2008). The thickness of glacimarine sediments, especially diatomaceous sediments, varies widely across the shelf, indicating differences in the rate of grounding-line retreat, rates of biogenic sediment production and preservation, and marine

current reworking of sediments (Dunbar et al., 1985; Cunningham et al., 1999).

Licht and Andrews (2002) and Mosola and Anderson (2006) established that cores from the eastern Ross Sea generally consisted of predominantly terrigenous glacimarine sediments resting in sharp contact on till. The absence of an upper diatomaceous facies in the central and eastern Ross Sea indicates the presence of widespread and persistent sea-ice cover that has restricted primary productivity (Dunbar et al., 1985; Mosola and Anderson, 2006).

The first paleo-drainage reconstructions for the LGM ice sheet assumed that ice streams had occupied bathymetric troughs on the shelf (Hughes, 1973). Anderson et al. (1983, 1992) used heavy minerals and clays in diamictites, interpreted to be either tills or proximal glacimarine sediments, to reconstruct ice-sheet paleo-drainage on the continental shelf. Their results are consistent with those of more detailed petrographic and geochemical provenance studies by Licht et al. (2005, 2006), Farmer et al. (2006) and Licht and Palmer (2013) that indicate both EAIS- and WAIS-sourced ice flowed into the Ross Sea during the LGM with convergence at ~180° longitude (Licht et al., 2005, 2006; Farmer et al., 2006; Licht and Palmer, 2013).

A major advance in understanding the glacial history of the Ross Sea, as well as other sectors of the Antarctic continental shelf, came with the development of multibeam swath bathymetry. Shipp et al. (1999, 2002) mapped geomorphological features including mega-scale glacial lineations (MSGL), grounding zone wedges (GZW), drumlins, grooves and megaflutes and iceberg furrows in the western Ross Sea (Figs. 3 and 4), and Mosola and Anderson (2006) and Bart and Cone (2012) subsequently mapped similar features in the central and eastern Ross Sea (Figs. 4 and 5). Based on the scale of the subglacial geomorphic features (several meters in amplitude)

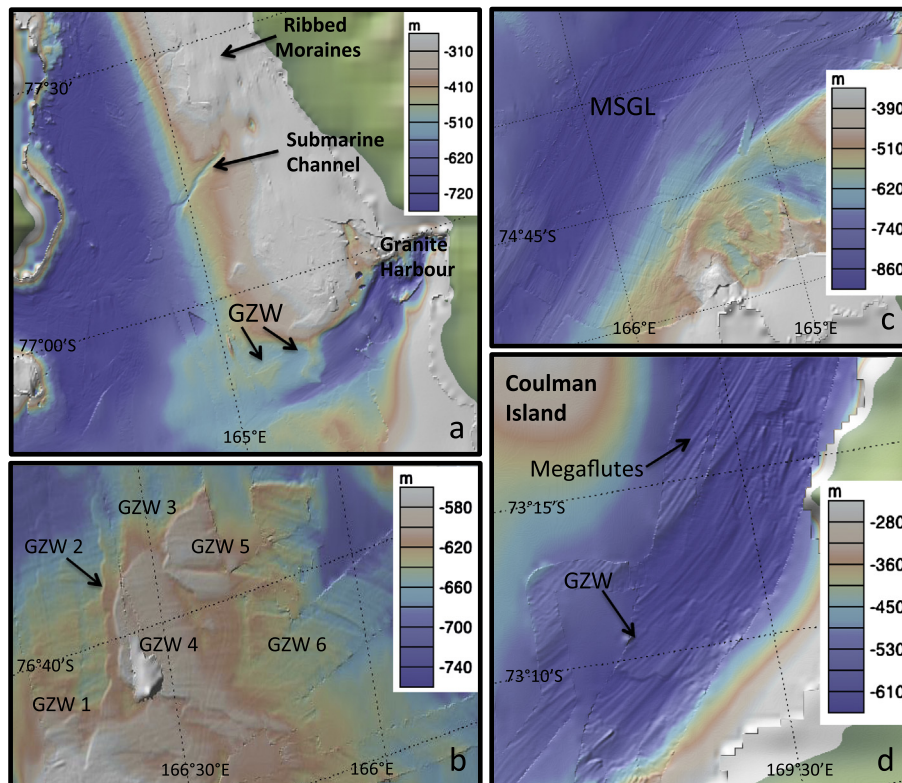


Fig. 3. Representative multibeam images from the western Ross Sea – locations of images are shown in Fig. 4. Color-scale represents bathymetry (m below present-day sea level). (a) McMurdo Sound area showing general lack of geomorphic features in deeper portion of sound, submarine channel on western flank of the sound and back-stepping grounding zone wedges (GZW) at the mouth of Granite Harbor, (b) back-stepping GZW indicate grounding line retreat from west to east north of Ross Island, (c) MSGL within northern Drygalski Trough, and (d) megaflutes and MSGL west of Coulman Island.

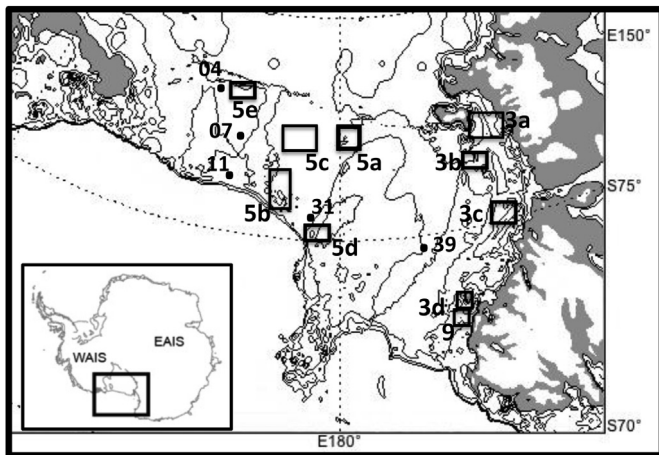


Fig. 4. Locations of multibeam images shown in Figs. 3 and 4. Also shown are the locations of sediment cores referred to in text using core numbers.

and relatively thin (typically less than 1 m) cover of glaciomarine sediments that overlie these features and tills, it is generally assumed that the geomorphic features formed during the most recent glacial advance onto the continental shelf. Results from these geomorphological studies are consistent with the provenance

studies. The combined data delineate the position and flow directions of paleo-ice streams draining the EAIS and WAIS (Fig. 6), which are generally consistent with those assumed by Hughes (1973). We caution that Fig. 6 is based strictly on provenance studies and the distribution of subglacial geomorphic features and hence it reflects the paleodrainage during maximum ice sheet expansion. As we will see, there is some evidence that the maximum expansion of the ice sheet was not contemporaneous across the Ross Embayment.

Onshore studies have shown that Minna Bluff, Ross Island, and other smaller volcanic islands exerted strong control on the ice-sheet-shelf system in the western Ross Sea (Stuiver et al., 1981; Denton and Marchant, 2000; Hall et al., 2013). Ice flowed north and south around Ross Island and from the east toward the west (Fig. 7). Ice that flowed north of Ross Island transported kenyte from the islands and deposited it in the mouths of Taylor Valley and in valleys fronting the Royal Society Range.

High-resolution swath bathymetry data provide further details about the paleo-glacial drainage in McMurdo Sound (Greenwood et al., 2012). From these data, four stages of ice-flow evolution are inferred: (i) northeastward flow into the Ross Sea from McMurdo Sound; (ii) westward flow from the Ross Sea around Ross Island and onto the Victoria Land coast; (iii) a deglacial phase with minor shifts in flow and grounding-line retreat into McMurdo Sound; (iv) grounding-line pinning on Ross Island during regional retreat.

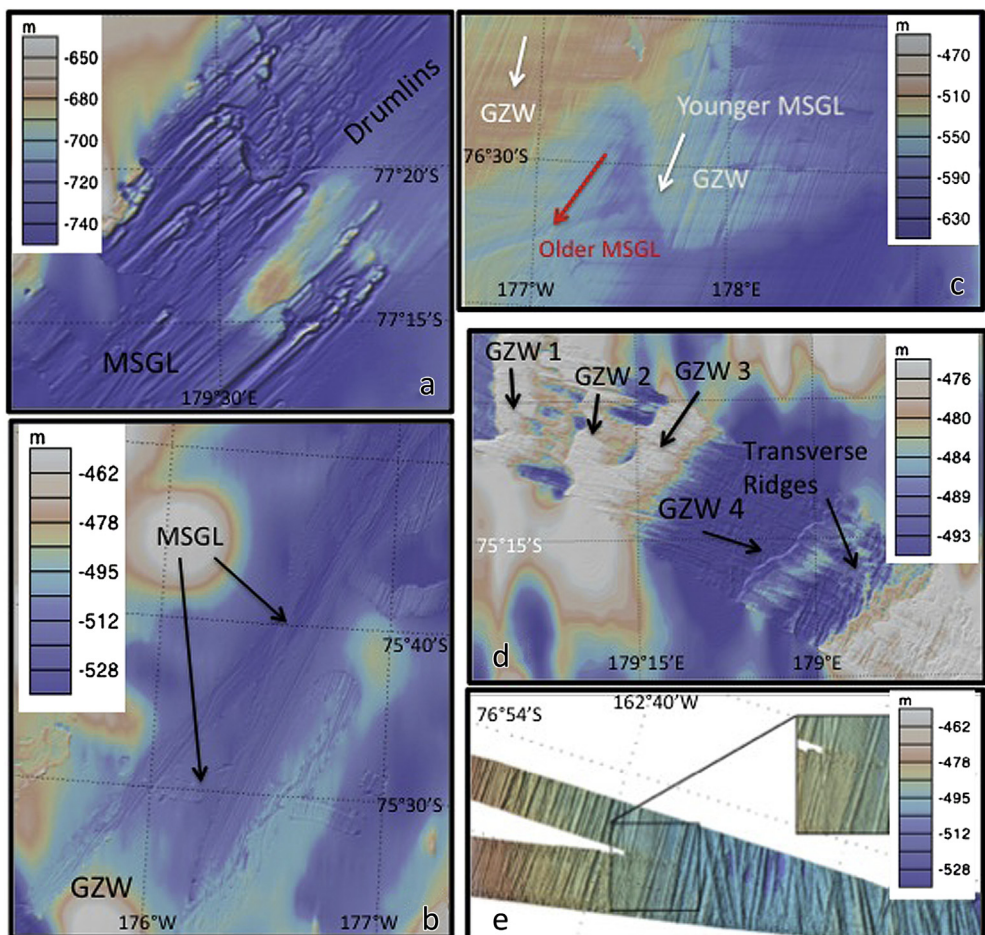


Fig. 5. Representative multibeam images from the eastern Ross Sea – locations of images shown in Fig. 2. Color-scale represents bathymetry (m below present-day sea level). (a) drumlin field within trough 4. (b) MSGL on outer shelf within trough 4. (c) grounding zone wedge overlying older MSGL and overprinted by younger set of MSGL with arrows highlighting different orientations of MSGL. (d) back-stepping grounding zone wedges (GZW) on western flank of Pennell Bank, and (e) high-resolution multibeam image showing corrugation ridges overprinted by iceberg furrows.

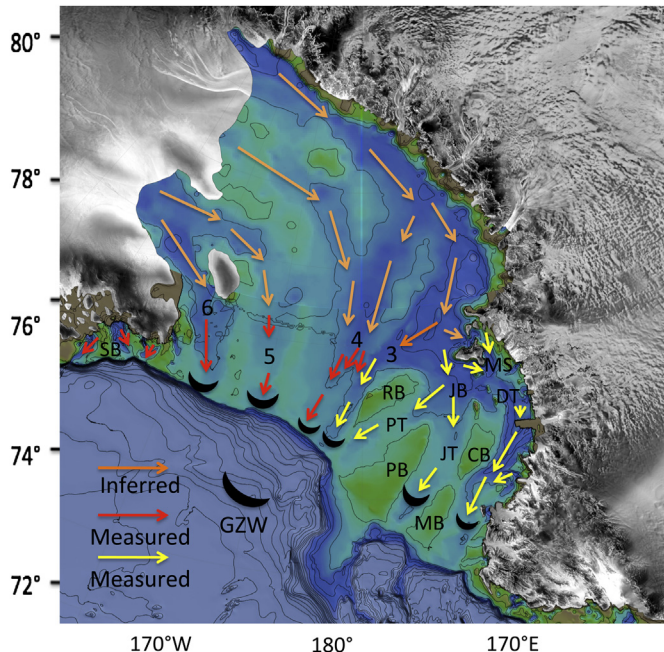


Fig. 6. Paleo-drainage map for the maximum ice sheet advance based on combined sediment provenance data and on the orientations of linear subglacial geomorphic features. The boundary between ice draining East Antarctica (yellow arrows) and ice draining West Antarctica (red arrows) is situated at approximately 180° longitude. There is evidence that expansion and retreat of the ice sheet from these areas may have been diachronous, so this reconstruction does not necessarily represent the LGM configuration of the ice sheet (see text). The orange arrows reflect inferred paleo-drainage in the area beneath the Ross Ice Shelf, which is based on locations of troughs. MS = McMurdo Sound, DT = Drygalski Trough, CB = Crary Bank, JB = JOIDES Basin (Trough), JT = JOIDES Trough, MB = Mawson Bank, PB = Pennell Bank, PT = Pennell Trough, RB = Ross Bank, SB = Sulzberger Bay and the numbers 3, 4, 5 and 6 correspond to the numbering system used by Mosola and Anderson (2006) to designate troughs. For more detailed descriptions and maps of geomorphic features see Shipp et al. (1999) and Mosola and Anderson (2006).

Scattered, obscure subglacial bedforms exist in the deeper portions of McMurdo Sound, suggesting that these features formed during an early episode of grounding and were partially buried by younger sediments. These features indicate flow to the north (Fig. 6). Bedforms along the northern margin of the sound indicate that the ice sheet flowed around Ross Island and to the west. While our paleo-drainage map shows both flow paths, Greenwood et al. (2012) suggest that westward flow occurred after the northeastward flow. Terrestrial landforms and chronologies from glacial deposits adjacent to McMurdo Sound discussed below indicate that westward flow predominated through the LGM.

North of Ross Island, a single trough divides into three separate troughs: Drygalski Trough, JOIDES Basin-Trough, and Pennell Trough (Fig. 6). Four prominent banks (Crary, Mawson, Pennell and Ross) separate the troughs on the western shelf (Fig. 6). Geomorphic features are sparse in Drygalski Trough south of the Drygalski Ice Tongue, but MSGL and megaflutes occur all along and within the deepest portions of the trough north of the ice tongue to the approximate location of Coulman Island (Fig. 3c,d). The inference is that EAIS outlet glaciers north of Ross Island discharged into Drygalski Trough where they merged into one large ice stream (Fig. 6). The outer shelf is characterized by less distinct lineations that are overprinted by iceberg furrows. Shipp et al. (1999) argued that a GZW just north of Coulman Island (Fig. 3d) marks the LGM grounding line. The ice sheet was grounded on the shallower portions of the continental shelf, including the shelf west of Cape Adare where subglacial geomorphic features occur in the deepest portions of troughs (Anderson et al., 2002).

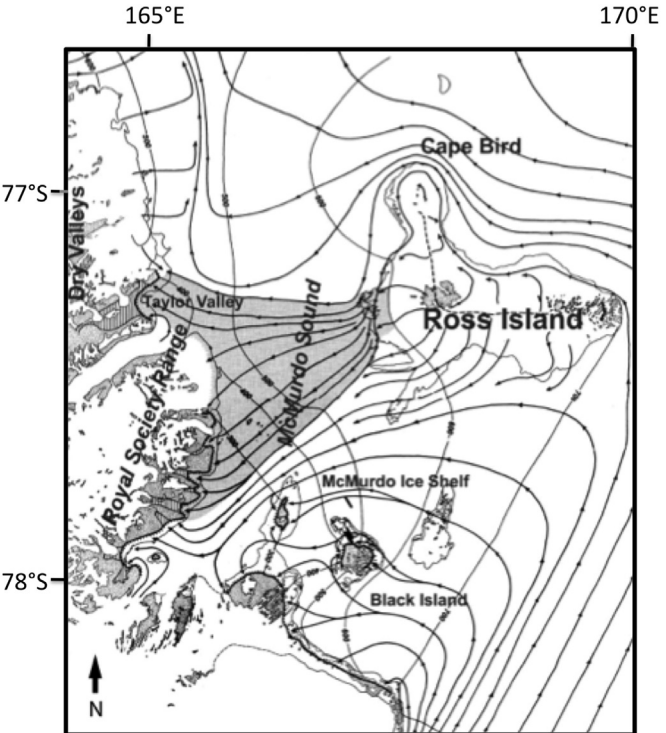


Fig. 7. Reconstruction of ice-flow lines in the McMurdo Sound region at the LGM (modified from Denton and Marchant, 2000). Ice flowed north and south around Ross Island from the east toward the west. Ice that passed north of Ross Island carried kenyte and deposited it in the mouth of Taylor Valley and in the valleys fronting the Royal Society Range (shaded band). Ice-dammed lakes occupied these valleys (diagonal pattern).

The shelf bathymetry indicates that ice flowed from the south into JOIDES Basin (Fig. 6). Although MSGL were not imaged in the southern portion of JOIDES Basin, deep-tow side-scan sonar records show small-scale lineations associated with back-stepping wedges that formed during the retreat of the grounding line from this portion of the trough (Shipp et al., 1999). Swath bathymetry collected from the outer portion of JOIDES Trough show MSGL that, similar to Drygalski Trough, do not extend to the shelf margin but rather terminate at a prominent outer shelf GZW. Thus, the grounding line does not appear to have extended to the shelf margin during the LGM (Licht et al., 1999; Shipp et al., 1999). This is supported by the occurrence of bioclastic carbonates on the outer portions of Mawson and Pennell Banks that have yielded LGM and pre-LGM radiocarbon ages (Taviani et al., 1993).

Licht and Palmer (2013) focused on tracing ice emanating from Byrd Glacier and found evidence that it flowed on either side of Ross Bank into the western and west-central Ross Sea. The confluence of East and West Antarctic derived ice occurs between Trough 3 and Trough 4 (Fig. 6). This conclusion is based on three difference provenance tracers. The newest dataset, using detrital zircons from glacial till, reveal distinctive signatures for Byrd Glacier (abundant 530 and 590 Ma grains) and West Antarctica (~100 Ma grains). Since the samples analyzed were in the top 1.5 m of till, the interpretation represents the later stages of grounded ice in this area. Multibeam records support the Licht and Palmer (2013) reconstruction and show two sets of MSGL that indicate flow around Ross Bank and into JOIDES Basin to the west and into trough 3 to the east (Fig. 6).

Few multibeam data have been collected within Pennell Trough, but Shipp et al. (1999) acquired deep-tow side-scan sonar records from the southern portion of the trough that show lineations

indicating flow toward the northeast. Multibeam images from the seaward portion of Pennell Trough show MSGL that extend seaward into a prominent shelf-margin GZW. Ice that flowed around the eastern side of Ross Bank sculpted a prominent drumlin field that extends seaward into MSGL (Fig. 5a). The MSGL terminate near the shelf margin in a GZW that is overprinted by iceberg furrows (Fig. 5b).

At approximately 180°W, the convergence of ice sourced in East Antarctica and interior West Antarctica is marked by two merging sets of MSGL within troughs 3 and 4 (Fig. 6). Shipp et al. (1999) originally mapped these as a single set, but data collected during later cruises clearly show two distinct sets of MSGL (Mosola and Anderson, 2006; Bart and Cone, 2012). The eastern set is oriented toward the northeast, parallel to the trough axis, and extends to within a few kms of the shelf margin (Fig. 5b). Another MSGL set occurs within trough 4 and displays two distinct orientations. An older set that has a more easterly orientation lies beneath a prominent mid-shelf GZW that is, in turn, overprinted by the younger more northerly oriented set of MSGL (Fig. 5c). Bart and Cone (2012) conducted a detailed study of this mid-shelf GZW and their results will be discussed later.

Trough 5 (Fig. 6) contains well-defined MSGL near the outer shelf and obscure MSGL on the inner shelf that are over-printed by iceberg furrows (Mosola and Anderson, 2006). A large GZW on the mid-shelf overlies MSGL that extend to the shelf margin where another GZW occurs. The eastern-most trough within the eastern Ross Sea (Trough 6, Fig. 6) contains well-developed MSGL that follow the curvature of the trough and extend to the shelf margin (Mosola and Anderson, 2006). To the east of the Ross Sea Embayment in Sulzberger Bay, drumlins, grooves and megaflutes carved into bedrock extend to the continental shelf break (Wellner et al., 2001).

2.1.2. Reconstruction of ice sheet minimum thickness in the marine sector

Estimates of the minimum ice-thickness on the continental shelf can be estimated using the bathymetry of the troughs where there is evidence that the ice sheet was grounded (Fig. 8). For a freely floating ice mass the relationship between elevation above sea level and ice thickness assuming hydrostatic equilibrium is:

$$\bar{\rho}_i H = \rho_w (H - h) \quad (1)$$

where $\bar{\rho}_i = 910 \text{ kg m}^{-3}$ and $\rho_w = 1028 \text{ kg m}^{-3}$ are the mean densities of the ice column and sea water, respectively, and H is ice thickness. An ice mass will be lightly grounded when the water depth $D = (H - h)$. Present-day water depth D comes from bathymetric data; where ΔD_{LGM} is the difference in sea level from today at the LGM (assumed to be -120 m). The minimum ice thickness during the LGM is derived using:

$$H_{\text{LGM}} = (\rho_w / \bar{\rho}_i) [D + \Delta D_{\text{LGM}}] \quad (2)$$

Estimated minimum values, shown in Fig. 7, need to be treated with caution for several reasons: (i) even lightly grounded ice is not in hydrostatic equilibrium; (ii) the mean density of ice sheets can vary widely (e.g. Shabtaie and Bentley, 1982); (iii) local values of ΔD_{LGM} were likely different from the global average value used here; and (iv) the calculation neglects isostatic effects.

The deepest grounding depth occurred in the Drygalski Trough; in order to be grounded the ice there had to be at least 1230 m thick during the LGM (Fig. 8). On the inner shelf in the central Ross Sea, where ice was grounded at water depths up to 760 m , the minimum ice thickness near the current ice shelf front would have been 812 m within Trough 3. The minimum thickness of the ice sheet at

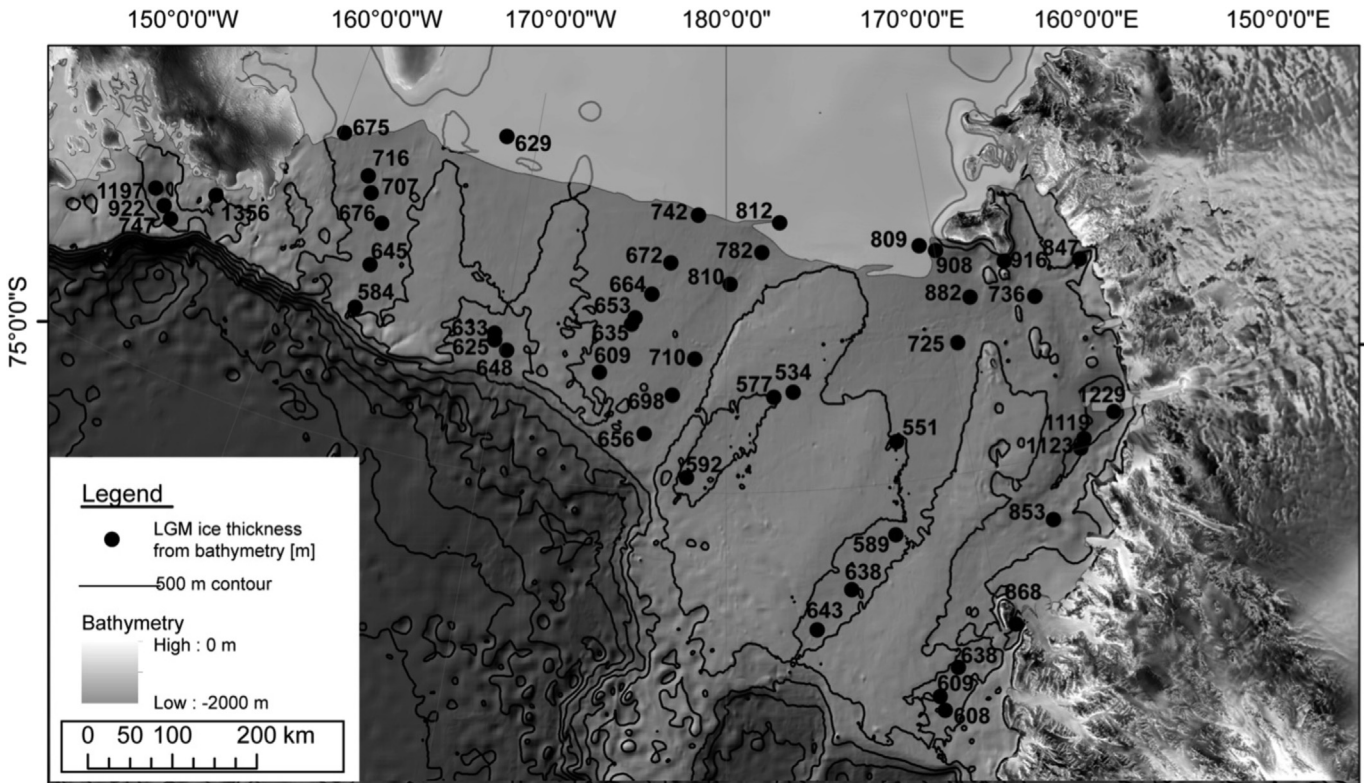


Fig. 8. Map showing points where minimum thickness for ice sheet were calculated, based on the presence of subglacial geomorphic features indicating that ice was grounded at these locations.

the outer continental shelf would have been between 580 m and 650 m. Farther east in Sulzberger Bay, the age of drumlins and megaflutes carved into bedrock is not known, but if these features formed during the LGM the minimum ice-thickness on the inner shelf would have been between 1200 m and 1350 m. In summary, minimum surface elevations of the grounded ice sheet during the LGM were 100 m–140 m above sea level at that time; surface elevations on the middle and outer shelf were close to present-day sea level.

2.2. Terrestrial geologic and glaciologic evidence: extent and thickness

Terrestrial evidence of ice-sheet thickness and extent during the LGM comes from (i) a widespread drift sheet (Ross Sea drift) with far-traveled erratics located on islands and peninsulas in the Ross Embayment, along the southern Scott Coast, and in the mouths of the Dry Valleys and the valleys fronting the Royal Society Range (Fig. 1); (ii) the occurrence of discontinuous, but correlative, drift sheets alongside EAIS outlet glaciers in the Transantarctic Mountains (TAM) from Reedy Glacier to Terra Nova Bay; (iii) relatively unweathered drift sheets deposited on nunataks in Marie Byrd Land and inland West Antarctica; (iv) results from glaciological models constrained by data from ice cores, radar-detected internal stratigraphy from ice rises, and visible flow features such as flow-stripes and crevasse patterns, that are often well preserved in the Ross ice streams and in the Ross Ice Shelf (Casassa et al., 1991; Merry and Whillans, 1993; Fahnestock et al., 2000).

Below we discuss terrestrial geologic and glaciologic evidence from the western, central and eastern Ross Embayment. Elevations here and elsewhere in the text are referenced to present-day sea level (asl), and are not corrected for isostatic changes.

Along the Northern Victoria Land coast, EAIS outlet glaciers that merged with grounded ice in the Ross Embayment deposited a widespread drift sheet (Terra Nova drift), which has been correlated to Ross Sea drift farther south on the basis of elevation, morphology, weathering, and limiting ages (Stuiver et al., 1981; Orombelli et al., 1990). Mapping of glacial geomorphologic features and reconstruction of the former longitudinal profile at Reeves Glacier near Terra Nova Bay indicate that the margin of the Ross Ice Sheet was ~400 m asl where it intersected the present-day coastline (Orombelli et al., 1990). EAIS outlet glaciers in the Dry Valleys region from Taylor to Victoria Valleys did not contribute to the Ross Sea Ice Sheet. Instead, tongues of westward-flowing ice advanced into eastern Taylor Valley and other valleys fronting the Royal Society Range (Péwé, 1960; Clayton-Greene et al., 1988; Denton and Hughes, 2000; Denton and Marchant, 2000; Hall et al., 2000) (Fig. 7). The grounded ice sheet deposited well-preserved moraines on headlands adjacent to McMurdo Sound, which allow reconstruction of former ice-surface elevations. Elevations of deposits marking the former ice margin range from ~720 m asl on eastern Ross Island, to >590 m asl on Cape Bird (Fig. 7), to 350–400 m asl at the mouth of Taylor Valley, and 250–300 m asl in front of the Royal Society Range (Stuiver et al., 1981; Dugel, 1985; Denton and Marchant, 2000; Dochat et al., 2000; Hall et al., 2000). Reconstructions of the slope of the former ice surface using moraine elevations indicate that most grounded ice in McMurdo Sound flowed westward around northern Ross Island and then south and west into the ice-free valleys on the mainland during the LGM (Fig. 7 – Stuiver et al., 1981; Denton and Marchant, 2000; Hall et al., 2000). This pattern of ice flow is consistent with the distribution of kenyte erratics in Ross Sea drift that were derived from western Ross Island.

A generally unweathered drift sheet, contrasting sharply with more distal weathered deposits, exists adjacent to many EAIS outlet

glaciers throughout the central and southern TAM. Based on its unweathered appearance, negligible soil development, and ice-cored nature in places, the origin of the drift is attributed to the LGM and Holocene deglaciation (Mercer, 1968; Bockheim et al., 1989; Denton et al., 1989a; Bromley et al., 2010, 2012). Reconstructions of past outlet-glacier extent show progressively less thickening up-glacier; changes in ice-surface elevations on the EAIS plateau were small during the LGM (Mercer, 1968; Bockheim et al., 1989; Denton et al., 1989a; Todd et al., 2010; Bromley et al., 2010, 2012). The former elevations of these glaciers where they entered the Ross Embayment afford estimates of surface elevation and thickness of the Ross Sea ice sheet. Mapping and ¹⁰Be exposure ages indicate that the elevation at the mouth of Reedy Glacier was 1100–1400 m asl during the LGM (Bromley et al., 2010; Todd et al., 2010). Evidence from Mt Rigby near the mouth of Scott Glacier and Taylor Ridge indicates the ice-sheet elevation was greater than 893 m, but less than 1200 m asl; our best estimate is 1000–1100 m asl (Bromley et al., 2012). Farther north, constraints from Mt Hope and Mt Kyffin at the mouth of Beardmore Glacier indicate elevations of 1080 m asl (Stone et al. unpublished), and at the Darwin/Hatherton Glacier system, it was 900–1100 m asl (Bockheim et al., 1989; Anderson et al., 2004).

The coastal Ford Ranges of Marie Byrd Land near the eastern margin of the Ross Embayment (Fig. 1) were overrun during the LGM, but exposure-ages from Mt Rea and The Billboard indicate the ice sheet was more than 800 m asl than present near the coast with less thickening farther inland (Stone et al., 2003). This pattern is consistent with expansion of the ice sheet to the edge of the continental shelf in Sulzberger Bay (Wellner et al., 2001). Farther inland in WAIS, LGM deposits have been recorded up to 45 m above present at Mt. Waesche (Ackert et al., 1999), and 125 m above present in the Ohio Range (Ackert et al., 2007, 2011).

Results from glaciological models constrained by ice-core data suggest a relatively low-profile ice sheet in the central Ross Embayment. Depth profiles of stable-isotopes from an ice core drilled on Siple Dome (Fig. 1), the inter-stream ridge between Kamb and Bindschadler Ice Streams, indicate the dome was not over-run during the LGM (Brook et al., 2005). In addition, Waddington et al. (2005) used the depth–age relationship from the core to establish a thickness history. The thickness of an annual layer $\lambda(t(z))$ of age t at depth z today is the product of the original layer thickness $b(t)$ when the snow was deposited (the ice-equivalent accumulation rate), and a dimensionless thinning function $\Lambda(z,t)$, which represents the cumulative effects of ice flow on the thickness of a particle as it travels along its path to depth z since it was deposited at time t in the past:

$$\lambda(t(z)) = \Lambda(z,t)b(t) \quad (3)$$

It follows that for a given accumulation history $b(t)$, a known depth–age relationship $t(z)$ or equivalently, an annual-layer thickness pattern $\lambda(t)$, allows just a single ice-sheet thickness history, because $\Lambda(z,t)$ depends on the ice-sheet thinning history; results using reasonable values for accumulation histories indicate that Siple Dome was 300–400 m thicker than present (900 m–1000 m asl) during the glacial maximum. Further, experiments using a thermo-mechanical ice-flow model of the ice streams surrounding the inter-stream ridges indicate thickening of ~100 m (200 m–300 m asl) during the LGM in the vicinity of the present-day grounding line (Parizek and Alley, 2004). The emerging evidence is consistent with the hypothesis that the Siple Coast ice streams likely slowed during the LGM, but they did not stagnate (Parizek et al., 2003).

In summary, the terrestrial data provide a consistent picture of ice-sheet thickness and extent during maximum glacial expansion.

Glacial geologic evidence from nunataks in the upper catchment regions of the Ross Sea sector in West Antarctica and alongside the upper reaches of outlet glaciers adjacent to the EAIS plateau indicates little thickening. In contrast, the expanded ice sheet thickened as much as 1000 m above present at the mouths of the southern and central TAM outlet glaciers; surface elevations there were 1100–1200 m asl. Glacial geologic evidence from the Ford Ranges on the eastern side of the Ross Embayment also indicates thickening, with the ice sheet reaching >800 m asl. In the central Siple Coast, models constrained by ice core data indicate that Siple Dome thickened to 900–1000 m asl, but it was not overrun by inland ice during the LGM. Farther north, the surface elevation of the ice sheet reached 720 m asl on the eastern side of Ross Island, but it decreased both to the west, where ice terminated at 250–400 m asl on the headlands of the Dry Valleys/Royal Society range, and to the north at Reeves Glacier near Terra Nova Bay where it was 400 m asl.

3. Paleodrainage during grounding line retreat

Generally, small geomorphic features: including GZW, recessional moraines and corrugation ridges that formed during retreat of the ice sheet: overprint the MSGL (Shipp et al., 1999; Mosola and Anderson, 2006; Bart and Cone, 2012; Jakobsson et al., 2011). GZW (Figs. 3 and 5) mark sites of deposition during extended pauses in grounding-line retreat. High-resolution seismic profiles and multibeam data collected along the axes of Ross Sea troughs show variable numbers and spacing of GZW and in several cases, superposition of wedges (Shipp et al., 1999; Howat and Domack, 2003; Mosola and Anderson, 2006; Bart and Cone, 2012; Bart and Owolana, 2012). Back-stepping wedges (Figs. 3a, 3b and 5d) record pauses in the grounding line position during retreat. Some wedges rest on and are overprinted by MSGL with different orientations (e.g. Fig. 5c). The data also show cross-cutting MSGL, indicating changes in the direction of flow through time (e.g. Fig. 5e). These observations indicate a complex history of grounding line migrations by different paleo-ice streams as the ice sheet retreated from the continental shelf.

Throughout the Ross Sea, iceberg furrows overprint and generally conceal other geomorphic features on more shallow banks, trough flanks and on the shelf margin. More linear and isolated iceberg furrows also occur in the deeper portions of the troughs and overprint GZW and MSGL (Fig. 5b), indicating that retreat of the ice sheet from the continental shelf was punctuated by calving at or near the grounding line (Shipp et al., 1999; Mosola and Anderson, 2006).

Recessional moraines (transverse ridges of Dowdeswell et al., 2008) occur in multiple sets and are oriented perpendicular to the ice-flow direction. They have amplitudes of 2–10 m and wavelengths of a few tens to hundreds of meters (Fig. 5d). Prominent sets of recessional moraines occur along the axis of JOIDES Trough, along the flanks of Crary Bank, Mawson Bank and Crary Bank, around the flank of Ross Island and along the southern flank of Trough 5 in eastern Ross Sea. It is thought that they formed by step-wise retreat of the grounding line (Dowdeswell et al., 2008), and some more-regularly spaced moraines may even reflect annual retreat of the grounding line (Shipp et al., 1999).

Corrugation ridges are distinguished from recessional moraines by their smaller wavelengths and more regular spacing. They are thought to record episodes of ice shelf collapse and associated rapid grounding-line retreat (Jakobsson et al., 2011). Corrugation ridges (Fig. 5e) were imaged in a number of locations where high-resolution swath bathymetry data have been collected in the southern Ross Sea (Shipp et al., 1999; Jakobsson et al., 2011), which suggests that they may be widespread on the shelf.

While the age of geomorphic features formed during the retreat of the ice sheet from the continental shelf is poorly constrained, these features indicate a complex pattern of grounding-line retreat with episodes of back-stepping of the grounding line into shallower water depths punctuated by periods of grounding line stability. In the western Ross Sea, recessional moraines that back-step across the flanks of banks (e.g. Fig. 5d) indicate that, after decoupling from the deep floor of troughs, the grounding-line migrated onto these banks and likely remained grounded there during the final stages of retreat (Shipp et al., 1999). Likewise, GZW on the shallow shelf just north of Terra Nova Bay record an episode of grounding line stability during the final phase of retreat toward the coast and a significant change from the more northerly ice flow direction indicated by MSGL in the deeper portions of the adjacent Drygalski Trough (Fig. 9).

One of the more complex areas, in terms of geomorphic features, is within and north of McMurdo Sound. Back-stepping GZW indicate grounding line retreat from east to west, perpendicular to the regional southwards retreat, and rather indicating retreat towards coastal EAIS outlets (Fig. 3a and b). These GZW are overprinted by E–W oriented lineations. Eastward flow (westward retreat) is directly opposite to westward flow closer to Ross Island, and/or would represent a complete reversal of a major flow set during the final stages of grounding line retreat.

Recessional moraines appear to be widespread on the western flank of the McMurdo Sound. Submarine channels that extend onto the basin floor cut into these moraines and likely reflect a late stage of turbidity current actively (Greenwood et al., 2012) (Fig. 3a). A volcanoclastic fan complex occurs on the western flank of Ross Island (Bartek and Anderson, 1991). Given that reconstructions based on land-based moraine elevations imply ice in the Sound was grounded during the LGM (Hall et al., 2013), current thinking is that these recessional moraines and submarine channels formed in the final stages of deglaciation (Greenwood et al., 2012).

4. Timing of LGM and Holocene deglaciation

4.1. Timing of Holocene retreat from the continental shelf

Carbonate material in Ross Sea sediments is sparse, so there continues to be strong reliance on AIO (Acid Insoluble Organic fraction) ages obtained from diatomaceous sediments. These ages

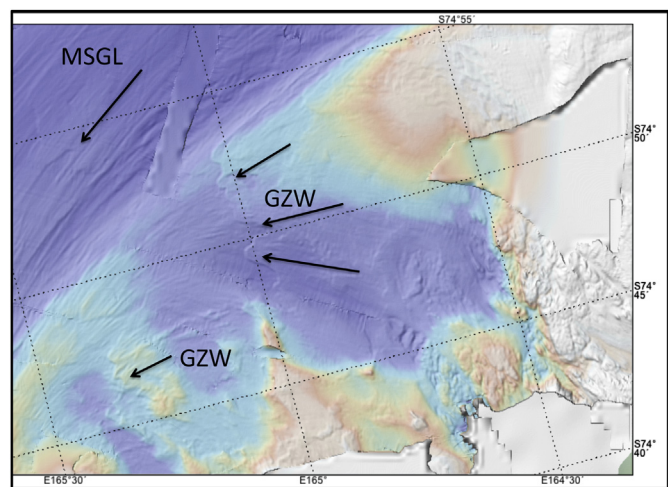


Fig. 9. Multibeam image from northern Drygalski Trough and adjacent inner shelf showing MSGL indicating northward flow and back-stepping GZW indicating flow toward the east and retreat to the west. See Fig. 4 for location.

Table 1

Table of all known radiocarbon dated material in the Ross Sea. See original reference for more information.

Reference	Lab no.	Ship	Cruise	Core type ^a	Core	Sample depth [cm]	$\delta^{13}\text{C}$	Age ^b yr BP	Error	Corrected age ^{b,c} cal yr BP	Latitude	Longitude	Water depth [mbf]	Core length [cm]	Lithology	Interpretation	Type of carbon
Bart and Cone, 2012	76652	Palmer	NBP08-02	PC	02	3–5	−27.45	4550	40	815	−76.53667	−177.55171	582		Pelagic	AIO	
Bart and Cone, 2012	76651	Palmer	NBP08-02	PC	02	7–9	−25.1	12,450	70	8715	−76.53667	−177.55171	582		Pelagic	AIO	
Bart and Cone, 2012	72191	Palmer	NBP08-02	PC	02	375–377	−20	36,800	560	33,065	−76.53667	−177.55171	582		Diamict	AIO	
Bart and Cone, 2012	72186	Palmer	NBP08-02	PC	02	356–422	0	32,400	840	31,200	−76.53667	−177.55171	582		Diamict	Foraminifera	
Bart and Cone, 2012	72192	Palmer	NBP08-02	PC	02	396–398	−20	40,900	2000	37,165	−76.53667	−177.55171	582		Diamict	AIO	
Bart and Cone, 2012	72187	Palmer	NBP08-02	PC	02	622–682	0	37,200	340	36,000	−76.53667	−177.55171	582		Diamict	Foraminifera	
Bart and Cone, 2012	72193	Palmer	NBP08-02	PC	02	640–642	−20	43,400	2800	39,665	−76.53667	−177.55171	582		Diamict	AIO	
Bart and Cone, 2012	72194	Palmer	NBP08-02	PC	02	662–664	−20	42,100	2100	38,365	−76.53667	−177.55171	582		Diamict	AIO	
Bart and Cone, 2012	76658	Palmer	NBP08-02	PC	07	0–2	−27.22	5060	35	1325	−76.40219	−177.29713	621		Pelagic	AIO	
Bart and Cone, 2012	76650	Palmer	NBP08-02	PC	07	4–6	−26.51	6480	50	2745	−76.40219	−177.29713	621		Pelagic	AIO	
Bart and Cone, 2012	72188	Palmer	NBP08-02	PC	07	216–274	0	32,400	650	31,200	−76.40219	−177.29713	621		Diamict	Foraminifera	
Bart and Cone, 2012	72195	Palmer	NBP08-02	PC	07	234–236	−20	38,900	880	35,165	−76.40219	−177.29713	621		Diamict	AIO	
Bart and Cone, 2012	72189	Palmer	NBP08-02	PC	07	346–376	0	31,800	730	30,600	−76.40219	−177.29713	621		Diamict	Foraminifera	
Bart and Cone, 2012	72196	Palmer	NBP08-02	PC	07	248–250	−20	42,900	1400	39,165	−76.40219	−177.29713	621		Diamict	AIO	
Bart and Cone, 2012	72197	Palmer	NBP08-02	PC	07	366–368	−20	39,700	1300	35,965	−76.40219	−177.29713	621		Diamict	AIO	
Bart and Cone, 2012	72190	Palmer	NBP08-02	PC	07	376–406	0	31,500	850	30,300	−76.40219	−177.29713	621		Diamict	Foraminifera	
Bart and Cone, 2012	72198	Palmer	NBP08-02	PC	07	386–388	−20	41,900	1300	38,165	−76.40219	−177.29713	621		Diamict	AIO	
Bart and Cone, 2012	76653	Palmer	NBP08-02	PC	01	0–2	−27.18	4470	40	735	−76.57832	−177.70163	571		Pelagic	AIO	
Bart and Cone, 2012	76654	Palmer	NBP08-02	PC	01	18.5–20.5	−26.6	6600	55	2865	−76.57832	−177.70163	571		Pelagic	AIO	
Bart and Cone, 2012	76655	Palmer	NBP08-02	PC	01	30–60	0	35,200	190	34,000	−76.57832	−177.70163	571		Diamict	Foraminifera	
Bart and Cone, 2012	76656	Palmer	NBP08-02	PC	10	0–2	−26.36	5690	45	1955	−76.45834	−178.43334	604		Pelagic	AIO	
Bart and Cone, 2012	76657	Palmer	NBP08-02	PC	10	13–15	−24.98	10,800	50	7065	−76.45834	−178.43334	604		Pelagic	AIO	
Brambati et al., 2002	GX24508							17,010	80	14,010					Maximum ice Extent in WRS	AIO	
Domack et al., 1999	AA-17351#	Palmer	NBP95-01	KC	39	0–1	−28.3	3140	50		−74.473	173.512	557	257	Diatom mud and ooze	Open marine	
Domack et al., 1999	AA-17355	Palmer	NBP95-01	KC	39	50–51	−28.9	4760	60		−74.473	173.512	557	257	Diatom mud and ooze	Open marine	
Domack et al., 1999	AA-17353	Palmer	NBP95-01	KC	39	100–101	−28.2	7020	60		−74.473	173.512	557	257	Diatom mud and ooze	Open marine	
Domack et al., 1999	AA-17356	Palmer	NBP95-01	KC	39	150–151	−28.4	7740	60		−74.473	173.512	557	257	Diatom mud and ooze	Open marine	
Domack et al., 1999	AA-17354	Palmer	NBP95-01	KC	39	190–192	−28.5	10,450	80		−74.473	173.512	557	257	Silt clay	Ice shelf	
Domack et al., 1999	AA-17352	Palmer	NBP95-01	KC	39	208–210	−26.7	14,290	95	13,010	−74.473	173.512	557	257	Muddy gravel	Ice retreat begins in wrs	
Domack et al., 1999	AA-17357#	Palmer	NBP95-01	KC	37	0–2	−24.4	2780	50		−74.498	167.743	924	173	Diatom mud and ooze	Open marine	
Domack et al., 1999	AA-17363	Palmer	NBP95-01	KC	37	10–11	−24.8	3020	50		−74.498	167.743	924	173	Diatom mud and ooze	Open marine	
Domack et al., 1999	AA-17358	Palmer	NBP95-01	KC	37	20–21	−25.3	4720	50		−74.498	167.743	924	173	Diatom mud and ooze	Open marine	
Domack et al., 1999	AA-17362	Palmer	NBP95-01	KC	37	30–31	−25.2	6210	55		−74.498	167.743	924	173	Diatom mud and ooze	Open marine	
Domack et al., 1999	AA-17359	Palmer	NBP95-01	KC	37	40–41	−26.8	8630	85		−74.498	167.743	924	173	Diatom mud and ooze	Open marine	
Domack et al., 1999	AA-17361	Palmer	NBP95-01	KC	37	55–56	−27.7	10,500	75		−74.498	167.743	924	173	Sandy diatom mud	Calving line	
Domack et al., 1999	AA-17360	Palmer	NBP95-01	KC	37	67–68	−26.6	13,840	95	12,930	−74.498	167.743	924	173	Silty clay	Distal ice shelf	
Domack et al., 1999	AA-17364#	Palmer	NBP95-01	KC	31	0–2	−23.7	2430	50		−75.7	165.417	879	210	Diatom mud and ooze	Open marine	
Domack et al., 1999	AA-17365	Palmer	NBP95-01	KC	31	9–11	−24.8	3140	50		−75.7	165.417	879	210	Diatom mud and ooze	Open marine	
Domack et al., 1999	AA-17366	Palmer	NBP95-01	KC	31	49–51	−24.8	5680	55		−75.7	165.417	879	210	Diatom mud and ooze	Open marine	
Domack et al., 1999	AA-17367	Palmer	NBP95-01	KC	31	116–118	−27.7	10,230	70		−75.7	165.417	879	210	Gray mud	Distal ice shelf	
Domack et al., 1999	AA-17368	Palmer	NBP95-01	KC	31	159–161	−26.9	12,280	95	11,270	−75.7	165.417	879	210	Muddy gravel with till granules	Proximal ice shelf	

(continued on next page)

Table 1 (continued)

Reference	Lab no.	Ship	Cruise	Core type ^a	Core	Sample depth [cm]	$\delta^{13}\text{C}$	Age ^b yr BP	Error	Corrected age ^{b,c} cal yr BP	Latitude	Longitude	Water depth [mbsf]	Core length [cm]	Lithology	Interpretation Type of carbon
Domack et al., 1999	AA-17369	Palmer	NBP95-01	PC	26	0–2	-26.0	2210	55	-76.977	162.89	800	892			
Domack et al., 1999	AA-17373	Palmer	NBP95-01	PC	26	140–141	-25.9	3460	55	-76.977	162.89	800	892			
Domack et al., 1999	AA-17372	Palmer	NBP95-01	PC	26	280–281	-26.4	4240	55	-76.977	162.89	800	892			
Domack et al., 1999	AA-17371	Palmer	NBP95-01	PC	26	610–611	-25.4	6070	65	-76.977	162.89	800	892			
Domack et al., 1999	AA-17368	Palmer	NBP95-01	PC	26	790–791	-26.8	7690	65	-76.977	162.89	800	892			
Domack et al., 1999	AA-19473	Palmer	NBP95-01	PC	29	50–51	-26.5	3900	65	-76.985	162.972	867	892			
Domack et al., 1999	AA-19474	Palmer	NBP95-01	PC	29	125–126	-25.0	4060	70	-76.985	162.972	867	892			
Domack et al., 1999	AA-19475	Palmer	NBP95-01	PC	29	290–291	-27.2	4320	95	-76.985	162.972	867	892			
Domack et al., 1999	AA-19476	Palmer	NBP95-01	PC	29	380–381	-25.7	5050	70	-76.985	162.972	867	892			
Domack et al., 1999	AA-19477	Palmer	NBP95-01	PC	29	430–431	-25.8	5090	70	-76.985	162.972	867	892			
Domack et al., 1999	AA-19478	Palmer	NBP95-01	PC	29	538–539	-26.6	5540	75	-76.985	162.972	867	892			
Domack et al., 1999	AA-19479	Palmer	NBP95-01	PC	29	652–653	-27.3	5770	75	3960						
Domack et al., 1999	AA-19480	Palmer	NBP95-01	TC	11	0–2	-27.1	4140	100	-76.453	-179.087	659	86			
Domack et al., 1999	AA-19481	Palmer	NBP95-01	TC	11	16–18	-26.0	7890	80	-76.453	-179.087	659	86			
Domack et al., 1999	AA-19482	Palmer	NBP95-01	TC	11	45–47	-24.1	22740	250	-76.453	-179.087	659	86			
Domack et al., 1999	AA-19492	Palmer	NBP95-01	TC	16	2–4	-25.0	4040	65	-76.943	-179.823	712	80			
Domack et al., 1999	AA-19491	Palmer	NBP95-01	TC	12	0–2	-26.8	4530	65	-76.785	-177.822	568	223			
Domack et al., 1999	AA-19483	Palmer	NBP95-01	TC	40	0–2	-27.9	4170	65	-74.473	173.507	556	40			
Domack et al., 1999	AA-19484	Palmer	NBP95-01	TC	40	24–26	-28.4	4540	65	-74.473	173.507	556	40			
Domack et al., 1999	AA-19485	Palmer	NBP95-01	TC	40	43–45	-27.5	5420	70	-74.473	173.507	556	40			
Domack et al., 1999	AA-17374 ^d	Palmer	NBP95-01	G	54	0	0.8	1090	45	-73.15	174.968	381	0			
Domack et al., 1999	AA-17375 ^d	Palmer	NBP95-01	G	54	0	1	1130	45	-73.15	174.968	381	0			
Domack et al., 1999	AA-19488	Palmer	NBP95-01	PC	49	90–91	-26.3	4480	120	-73	171.743	607	98			
Domack et al., 1999	AA-19489	Palmer	NBP95-01	PC	49	65–66	-26.8	5280	75	-73	171.743	607	98			
Domack et al., 1999	AA-13975	Palmer	NBP94-01	PC	1	2–5	2850	50	-77.194	167.888	939	268				
Domack et al., 1999	AA-13976	Palmer	NBP94-01	PC	1	16–18	31450	475	-77.194	167.888	939	268				
Domack et al., 1999	AA-13977	Palmer	NBP94-01	PC	1	0–2	2580	55	-77.194	167.888	939	268				
Domack et al., 1999	AA-13978	Palmer	NBP94-01	PC	1	11–12	2680	50	-77.194	167.888	939	268				
Domack et al., 1999	AA-13979	Palmer	NBP94-01	PC	1	29–31	3250	55	-77.194	167.888	939	268				
Domack et al., 1999	AA-13970	Palmer	NBP94-01	TC	16	0–1	4410	50	-74.652	174.57	465	0	Gray diatomaceous mud and ooze	Open marine		
Domack et al., 1999	AA-13971	Palmer	NBP94-01	TC	16	15–16	11,660	90	-74.652	174.57	465	0	Gray diatomaceous mud and ooze	Open marine		
Domack et al., 1999	AA-13972	Palmer	NBP94-01	TC	16	30–31	13,380	85	-74.652	174.57	465	0	Granulated facies	Ice shelf		
Domack et al., 1999	AA-13973	Palmer	NBP94-01	TC	16	45–46	18,010	125	-74.652	174.57	465	0	Diamicton	Subglacial		
Domack et al., 1999	AA-13974	Palmer	NBP94-01	TC	16	53–55	32,520	475	-74.652	174.57	465	0	Diamicton	Subglacial		
Domack et al., 1999	AA-13942	Palmer	NBP94-01	PC	17	4–6	3690	70	-74.49	173.801	556	366				
Domack et al., 1999	AA-13943	Palmer	NBP94-01	PC	17	10–12	30,210	410	-74.49	173.801	556	366				
Domack et al., 1999	AA-13944	Palmer	NBP94-01	TC	17	0–2	33,40	45	-74.49	173.801	556	48				
Domack et al., 1999	AA-13945	Palmer	NBP94-01	TC	17	14–16	44,80	50	-74.49	173.801	556	48				
Domack et al., 1999	AA-13946	Palmer	NBP94-01	TC	17	24–26	5170	50	-74.49	173.801	556	48				
Domack et al., 1999	AA-13947	Palmer	NBP94-01	TC	17	34–36	5700	50	-74.49	173.801	556	48				
Domack et al., 1999	AA-13948	Palmer	NBP94-01	TC	17	44–46	6510	45	-74.49	173.801	556	48				
Domack et al., 1999	AA-13949	Palmer	NBP94-01	TC	18	0–2	4440	60	-74.383	173,304	560	53	Gray diatomaceous mud and ooze	Open marine		
Domack et al., 1999	AA-13950	Palmer	NBP94-01	TC	18	14–16	11,320	80	-74.383	173,304	560	53	Brown diatomaceous mud and ooze	Open marine		
Domack et al., 1999	AA-13951	Palmer	NBP94-01	TC	18	26–27	14,620	100	-74.383	173,304	560	53	Gravel and sand layer	Open marine		
Domack et al., 1999	AA-13952	Palmer	NBP94-01	TC	18	37–39	20,020	230	-74.383	173,304	560	53	Gravel and sand layer	Open marine		
Domack et al., 1999	AA-13961	Palmer	NBP94-01	TC	20	0–2	3580	50	-74,292	172,863	513	77				
Domack et al., 1999	AA-13962	Palmer	NBP94-01	TC	20	11–12	5980	60	-74,292	172,863	513	77				
Domack et al., 1999	AA-13963	Palmer	NBP94-01	TC	20	25–26	8950	70	-74,292	172,863	513	77				
Domack et al., 1999	AA-13964	Palmer	NBP94-01	TC	20	38–40	13,120	90	-74,292	172,863	513	77				
Domack et al., 1999	AA-13965	Palmer	NBP94-01	TC	20	45–47	18,370	140	-74,292	172,863	513	77				
Domack et al., 1999	AA-13987	Palmer	NBP94-01	TC	30	0–3	4620	100	-74,647	-179,636	628	81				

Domack et al., 1999	AA-13988	Palmer	NBP94-01	TC	30	23–24.5	20,530	200	–76,647	–179,636	628	81
Domack et al., 1999	AA-13989	Palmer	NBP94-01	TC	30	40–42	22,170	230	–76,647	–179,636	628	81
Domack et al., 1999	AA-13990	Palmer	NBP94-01	TC	30	65–67	33,550	655	–76,647	–179,636	628	81
Domack et al., 1999	AA-13953	Palmer	NBP94-01	PC	31	0–1	3240	50	–75,165	178,548	473	188
Domack et al., 1999	AA-13954	Palmer	NBP94-01	PC	31	10–11	4720	55	–75,165	178,548	473	188
Domack et al., 1999	AA-13955	Palmer	NBP94-01	PC	31	22–23	6640	60	–75,165	178,548	473	188
Domack et al., 1999	AA-13956	Palmer	NBP94-01	PC	31	36–38	16,530	125	–75,165	178,548	473	188
Domack et al., 1999	AA-20076	Palmer	NBP94-01	PC	31	100–101	30,000	480	–75,165	178,548	473	188
Domack et al., 1999	AA-20075	Palmer	NBP94-01	PC	31	140–142.5	31,140	470	–75,165	178,548	473	188
Domack et al., 1999	AA-13957	Palmer	NBP94-01	TC	31	0–2	3270	50	–75,165	178,548	473	72
Domack et al., 1999	AA-13958	Palmer	NBP94-01	TC	31	35–36	6090	55	–75,165	178,548	473	72
Domack et al., 1999	AA-13959	Palmer	NBP94-01	TC	31	50–51	8170	65	–75,165	178,548	473	72
Domack et al., 1999	AA-13960	Palmer	NBP94-01	TC	31	60–62	11,850	80	–75,165	178,548	473	72
Domack et al., 1999	AA-13991 ^g	Palmer	NBP94-01	TC	32	1–2.5	650	95	–75,3	179,39	489	63
Domack et al., 1999	AA-13966	Palmer	NBP94-01	TC	33	0–2	3370	50	–75,455	–179,615	603	92
Domack et al., 1999	AA-13967	Palmer	NBP94-01	TC	33	10–11.5	4310	70	–75,455	–179,615	603	92
Domack et al., 1999	AA-13968	Palmer	NBP94-01	TC	33	18–19	8130	60	–75,455	–179,615	603	92
Domack et al., 1999	AA-13969	Palmer	NBP94-01	TC	33	25–27	12,700	95	–75,455	–179,615	603	92
Domack et al., 1999	QL-1443						6450	90	7420			
Hall and Denton 1999	AA26500						5490	55	6290			
Hall and Denton 1999	AA26515						5540	50	6300			
Hall and Denton 1999	AA18912						5480	56	6280			
Hall and Denton 1999	AA20712						5350	60	6170			
Hall and Denton 1999	AA26514						5275	60	5990			
Hall and Denton 1999	AA14039						5250	97	5965			
Licht et al., 1996	AA-9361	Glacier	DF87	PC	32	80–84.5	27,720	340	26,520	–77,452	166,072	823
Licht et al., 1996	CAMS 4062	Glacier	DF87	PC	32	18–20	23,590	240	22,190	–77,452	166,072	823
Licht et al., 1996	AA17397	Palmer	NBP95-01	KC	34	13	1340	185	140	–75,165	164.5	1257
Licht et al., 1996	AA17401	Palmer	NBP95-01	KC	39	Top	1270	45	70	–74,473	173,512	557
Licht et al., 1996	AA11876	Glacier	DF80	PC	57	43	7330	60	6330	–77,283	165,817	869
Licht et al., 1996	CAMS 7789	Glacier	DF80	PC	57	0–2	3040	70	1840	–77,283	165,817	869
Licht et al., 1996	AA13244	Glacier	DF80	PC	102	0–7	4025	55	2825	–75,2	163,717	1116
Licht et al., 1996	CAMS 12581	Glacier	DF80	PC	102	90	12,640	80	11,440	–75,2	163,717	1116
Licht et al., 1996											231	Mud
Licht et al., 1996											130	Mud
Licht et al., 1996											130	Open water
Licht et al., 1996											core top	
Licht et al., 1996											core top	
Licht et al., 1996											Minimum age	

(continued on next page)

Table 1 (*continued*)

Reference	Lab.no.	Ship	Cruise	Core type ^a	Core	Sample depth [cm]	$\delta^{13}\text{C}$	Age ^b yr BP	Error cal yr BP	Corrected age ^{b,c} cal yr BP	Latitude	Longitude	Water depth [mbstf]	Core length [cm]	Lithology	Interpretation	Type of carbon
Licht et al., 1996	AA13242	Glacier	DF80	PC	108	22–26	11,545	95	10,345	–75,067	166	915	171	Mud	Minimum age AIO		
Licht et al., 1996	CAMS 8253	Glacier	DF80	PC	111	10–12	4750	70	3550	–74,917	167,483	554	120	Mud	Deglaciation	AIO	
Licht et al., 1996	CAMS 4061	Glacier	DF80	PC	112	5–6.5	5390	70	4190	–74,917	166,817	713	135	Mud	Open water	AIO	
Licht et al., 1996	CAMS 11793	Glacier	DF80	PC	132	62–65	10,730	80	9530	–75.55	166,133	668	230	Mud	Open water	AIO	
Licht et al., 1996	CAMS 8251	Glacier	DF80	PC	132	45–47	8390	80	7190	–75.55	166,133	668	230	Mud	Open water	AIO	
Licht et al., 1996	AA 17399	Glacier	DF80	PC	144	200	32,685	610	31,485	–73,017	172,167	457	219	Glaci. marine dianicton	Ice proximal	Glob. subglobosa	
Licht et al., 1996	AA11877	Glacier	DF80	PC	144	8–11	895	50	Modern	–73,017	172,167	457	219	Muddy sand	Open marine	Acyonian coral	
Licht et al., 1996	AA12899	Glacier	DF80	PC	144	13–14	21,255	200	20,055	–73,017	172,167	457	219	Glaci. marine dianicton	Ice proximal	Three sp. forams	
Licht et al., 1996	AA17398	Glacier	DF80	PC	144	10	12,890	105	11,690	–73,017	172,167	457	219	Muddy sand	Partially reworked	Glob. subglobosa	
Licht et al., 1996	CAMS 11798	Glacier	DF80	PC	144	8–11	6330	80	9530	–73,017	172,167	457	219	Muddy sand	Open marine	AIO	
Licht et al., 1996	CAMS 12582	Glacier	DF80	PC	144	21–24	22,360	140	21,160	–73,017	172,167	457	219	Glaci. marine dianicton	Ice proximal	AIO	
Licht et al., 1996	AA11878	Glacier	DF80	PC	177	230–233	27,255	305	26,055	–73,683	171,817	529	281	Glaci. marine dianicton	Ice proximal	Mixed forams	
Licht et al., 1996	AA13229	Glacier	DF80	PC	177	270	30,70	475	28,970	–73,683	171,817	529	281	Glaci. marine dianicton	Ice proximal	Three sp. forams	
Licht et al., 1996	AA15699	Glacier	DF80	PC	177	30	24,835	240	23,635	–73,683	171,817	529	281	Glaci. marine dianicton	Ice proximal	Two sp. benthics	
Licht et al., 1996	CAMS 7790	Glacier	DF80	PC	177	0–3	7470	70	6270	–73,683	171,817	529	281	Sandy mud	Open water, core top	AIO	
Licht et al., 1996	AA13243	Glacier	DF80	PC	189	111–115	7330	65	6130	–77.2	167,883	907	193	Massive mud	Open water	AIO	
Licht et al., 1996	CAMS 8252	Glacier	DF80	PC	189	9–10	2660	70	1460	–77.2	167,883	907	193	Massive mud	Open water	AIO	
Salvi et al., 2006	ANTA96-5bis	ANTA96-5bis	ANTA96-5bis	ANTA96-5bis	ANTA96-5bis	0–2	–30.6	3820	40	–75,4733333	–179,75917	568	636	Siliceous mud/ooze			
Salvi et al., 2006	ANTA96-5bis	ANTA96-5bis	ANTA96-5bis	ANTA96-5bis	ANTA96-5bis	90–92	–25.8	24,740	110	–75,7473333	–179,75917	568	636	sgf			
Salvi et al., 2006	ANTA96-5bis	ANTA96-5bis	ANTA96-5bis	ANTA96-5bis	ANTA96-5bis	190.5–192	–25.4	21,820	210	–75,7473333	–179,75917	568	636	sgf			
Salvi et al., 2006	ANTA96-5bis	ANTA96-5bis	ANTA96-5bis	ANTA96-5bis	ANTA96-5bis	339–342	–25.0	27,270	410	–75,7473333	–179,75917	568	636	sgf			
Salvi et al., 2006	ANTA96-5bis	ANTA96-5bis	ANTA96-5bis	ANTA96-5bis	ANTA96-5bis	450–453	–26.1	37,000	1400	–75,7473333	–179,75917	568	636	Glaci. Marine Diamicton			
Licht and Andrews, 2002	AA23222	Palmer	NBP95-01	PC	7	63–66	0.8	14,970	135	13,770	–75,625	–178,587	449	145	Stratified dianicton	Reworked ice proximal	Benth. forams
Licht and Andrews, 2002	AA23405	Palmer	NBP95-01	PC	7	2–4	–25.1	22,975	210	18,975	–75,625	–178,587	449	145	Stratified dianicton	Glaci. marine proximal	
Licht and Andrews, 2002	AA23406	Palmer	NBP95-01	PC	7	21–22	–25	25,695	300	21,695	–75,625	–178,587	449	145	Stratified dianicton	Reworked ice proximal	AIO
Licht and Andrews, 2002	AA23407	Palmer	NBP95-01	PC	7	63–66	–25.5	20,780	220	16,780	–75,625	–178,587	449	145	Stratified dianicton	Glaci. marine proximal	
Licht and Andrews, 2002	AA23417	Palmer	NBP95-01	PC	7	20–22	17,790	195	16,590	–75,625	–178,587	449	145	Stratified dianicton	Reworked ice proximal	Benth. forams	
Licht and Andrews, 2002	AA23418	Palmer	NBP95-01	PC	7	2–4	21,980	290	20,780	–75,625	–178,587	449	145	Stratified dianicton	Glaci. marine proximal		
Licht and Andrews, 2002	AA23408	Palmer	NBP95-01	PC	11	3–5	–26.6	6640	110	2640	–76,453	–179,087	659	165	Stratified dianicton	Glaci. marine Open marine	AIO
Licht and Andrews, 2002	AA23409	Palmer	NBP95-01	PC	11	61–63	–24.7	27,120	305	23,120	–76,453	–179,087	659	165	Massive dianicton	Subglacial, max age of ice advance	AIO

Licht and Andrews, 2002	AA23410	Palmer	NBP95-01	PC	17	2–4	–24.1	21.835	225	17.835	–77.452	179.05	732	202	Massive diamict	Subglacial, max age of ice advance
Licht and Andrews, 2002	AA23411	Palmer	NBP95-01	PC	18	10–12	n/a	17.760	115	14.025	–77.333	179.537	819	55	Mud with dropstones	ice proximal glacial
Licht and Andrews, 2002	AA23412	Palmer	NBP95-01	PC	18	21.5–23.5	–24.6	27.580	325	23.845	–77.333	179.537	819	55	Stratified diamict	marine, likely 'too old' ice proximal glacial
Licht and Andrews, 2002	AA23413	Palmer	NBP95-01	PC	18	41–43	n/a	25.870	245	22.135	–77.333	179.537	819	55	Stratified diamict	marine, likely 'too old' ice proximal glacial
Licht and Andrews, 2002	AA27801	Palmer	NBP95-01	TC	18	0–2	–28.7	37.35	60	0	–77.333	179.537	819	72	Gray or brown mud	Open water, core top
Licht and Andrews, 2002	AA27802	Palmer	NBP95-01	TC	18	26–28	–23.7	20.490	260	16.755	–77.333	179.537	819	72	Bioturbated mud with dropstones	Open marine, likely 'too old'
Licht and Andrews, 2002	AA27803	Palmer	NBP95-01	TC	18	62–64	–24	24.680	490	20.945	–77.333	179.537	819	72	Subice shelf, likely 'too old'	Subice shelf, ice proximal glacial
Licht and Andrews, 2002	AA23414	Palmer	NBP95-01	PC	24	4–6	–25.4	24.090	205	20.090	–76.607	–175.417	585	183	Stratified diamict	marine, likely 'too old' ice proximal glacial
Licht and Andrews, 2002	AA23415	Palmer	NBP95-01	PC	24	55–58	–25.2	31.310	480	27.310	–76.607	–175.417	585	183	Stratified diamict	ice advance
Licht and Andrews, 2002	AA23416	Palmer	NBP95-01	PC	24	105–107	–25.2	30.635	445	26.635	–76.607	–175.417	585	183	Stratified diamict	Subglacial, ice advance
Licht and Andrews, 2002	AA12114	Palmer	NBP94-01	PC	36	88–90	–24.5	30.220	420	26.220	–75.822	–177.224	622	96	Massive diamict	Subglacial, ice proximal glacial
Licht and Andrews, 2002	AA21761	Palmer	NBP94-01	TC	36	9–11	–25.6	13.830	90	9830	–75.823	–177.224	622	62	Sandy diamict	Subglacial, ice proximal glacial
Licht and Andrews, 2002	AA21762	Palmer	NBP94-01	TC	36	49–51	–24.8	30.510	415	26.510	–75.823	–177.224	622	62	Massive diamict	Subglacial, ice proximal glacial
Licht and Andrews, 2002	AA21763	Palmer	NBP94-01	PC	36	6–8	–24.8	26.955	340	22.955	–75.822	–177.224	622	96	Massive diamict	Subglacial, ice proximal glacial
Licht and Andrews, 2002	AA23224	Palmer	NBP94-01	TC	36	33–35	–24.7	28.055	315	24.055	–75.823	–177.224	622	62	Massive diamict	Subglacial, ice proximal glacial
McKay et al., 2008	NZA26112	Glacier	DF80	PC	78	224–226	–23.3	22.510	120	NA	–77.133	165.75	827	228	Diatomaceous ooze with limestones	Subglacial, ice proximal glacial
McKay et al., 2008	NZA25999	Glacier	DF80	PC	79	24–26	–25.2	18.613	85	NA	–77.467	165.683	845	216	Diatomaceous ooze with limestones	Subglacial, ice proximal glacial
McKay et al., 2008	NZA26000	Glacier	DF80	PC	79	109–111	–24.3	17.667	75	NA	–77.467	165.683	845	216	Diatomaceous ooze with limestones	Subglacial, ice proximal glacial
McKay et al., 2008	NZA25912	Glacier	DF80	PC	133	136–138	–26	8024	35	NA	–77.083	166.167	897	258	Diatomaceous ooze with limestones	Subglacial, ice proximal glacial
McKay et al., 2008	NZA26113	Glacier	DF80	PC	138	6–8	–24.2	26.310	180	NA	–77.183	167.617	914	254	Diatomaceous ooze with limestones	Subglacial, ice proximal glacial
McKay et al., 2008	NZA26114	Glacier	DF80	PC	138	143–145	–23.9	30.930	320	NA	–77.183	167.617	914	254	Diatomaceous ooze with limestones	Subglacial, ice proximal glacial
McKay et al., 2008	NZA26111	Glacier	DF80	PC	138	244–246	–25.9	20.780	100	NA	–77.183	167.617	914	254	Diatomaceous ooze with limestones	Subglacial, ice proximal glacial
McKay et al., 2008	NZA25941	Glacier	DF80	PC	189	7–9	–27.7	2470	35	0	–77.2	167.883	907	193	Diatomaceous ooze with limestones	Subglacial, ice proximal glacial
McKay et al., 2008	NZA25939	Glacier	DF80	PC	189	96–98	–26.7	7168	35	4698	–77.2	167.883	907	193	Diatomaceous ooze with limestones	Subglacial, ice proximal glacial
McKay et al., 2008	NZA25913	Glacier	DF80	PC	189	127–129	–25.2	11.331	45	8861	–77.2	167.883	907	193	Clast rich diamict	Subglacial, ice proximal glacial
McKay et al., 2008	NZA25940	Glacier	DF80	PC	189	176–178	–16.5	21.830	120	NA	–77.2	167.883	907	193	Clast rich diamict	Subglacial, ice proximal glacial
McKay et al., 2008	NZA18135	HotWaterDrill	HWD03	HWD	03-1	0–1	–27.2	4343	55	0	–77.88846667	167.08445	9999	9999	Interbedded mud and fine sandy mud	Sub-ice shelf mud/sand
McKay et al., 2008	NZA18846	HotWaterDrill	HWD03	HWD	03-1	04–05	–25.2	3845	35	1502	–77.88846667	167.08445	9999	9999	Interbedded mud/sand	Sub-ice shelf mud/sand

(continued on next page)

Table 1 (continued)

Reference	Lab no.	Ship	Cruise	Core type ^a	Core	Sample depth [cm]	$\delta^{13}\text{C}$	Age ^b yr BP	Error	Corrected age ^{b,c} cal yr BP	Latitude	Longitude	Water depth [mbsf]	Core length [cm]	Lithology	Interpretation	Type of carbon
McKay et al., 2008	NZA 18136	HotWaterDrill	HWD03	HWD	03-1	20–21	–24.9	18,080	100	13,737	–77,884,6667	167,08445	9999	9999	Interbedded mud and fine sandy mud	Sub-ice shelf mud/sand	
McKay et al., 2008	NZA 18137	HotWaterDrill	HWD03	HWD	03-1	33–34	–23.1	24,550	190	NA	–77,884,6667	167,08445	9999	9999	Clast rich muddy diamicton	Sub-ice shelf diamict	
McKay et al., 2008	NZA 18856	HotWaterDrill	HWD03	HWD	03-1	45–46	–22.6	25,750	190	NA	–77,884,6667	167,08445	9999	9999	Clast rich muddy diamicton	Sub-ice shelf diamict	
McKay et al., 2008	NZA 18857	HotWaterDrill	HWD03	HWD	03-1	58–59	–25	22,550	170	NA	–77,884,6667	167,08445	9999	9999	Clast rich muddy diamicton	Sub-ice shelf diamict	
McKay et al., 2008	NZA 18138	HotWaterDrill	HWD03	HWD	03-2	1–2.5	–26.9	2701	50	0	–77,835,18333	167,336817	9999	9999	Sandy mud	Sub-ice shelf boundary	
McKay et al., 2008	NZA 18847	HotWaterDrill	HWD03	HWD	03-2	9–10	–25.3	4743	40	2042	–77,835,18333	167,336817	9999	9999	Silty clay	Sub-ice shelf boundary	
McKay et al., 2008	NZA 18139	HotWaterDrill	HWD03	HWD	03-2	28–29	–25.7	5562	45	3861	–77,835,18333	167,336817	9999	9999	Silty clay/	Sub-ice shelf boundary	
McKay et al., 2008	NZA 18140	HotWaterDrill	HWD03	HWD	03-2	58–59	–25	12,797	85	10,096	–77,835,18333	167,336817	9999	9999	Glaciogenic boundary	Sub-ice shelf boundary	
McKay et al., 2008	NZA25403	HotWaterDrill	HWD06-3	HWD	06-3	1–3	–28	4675	40	NA	–77,9168	167,309	9999	9999	Clast rich muddy diamicton	Sub-ice shelf diamict	
McKay et al., 2008	NZA25420	HotWaterDrill	HWD06-3	HWD	06-3	31–33	–24.3	10,982	60	NA	–77,9168	167,309	9999	9999	Clast rich muddy diamicton	Sub-ice shelf diamict	
Mosola and Anderson, 2006	AA49685	Palmer	NBF99-02	TC	3	3–5	–26.1	8959	53	5224	–77,584	–177,834	667	65	Glacial marine mud	Open water AIO	
Mosola and Anderson, 2006	AA49686	Palmer	NBF99-02	TC	3	10–12	–24.9	22,600	220	18,865	–77,584	–177,834	667	65	Glacial marine mud	Open water AIO	
Mosola and Anderson, 2006	AA49687	Palmer	NBF99-02	TC	3	30–32	–24.8	20,520	130	16,785	–77,584	–177,834	667	65	Glacial marine mud	Open water AIO	
Mosola and Anderson, 2006	AA49688	Palmer	NBF99-02	TC	3	46–48	–23.9	30,440	390	26,705	–77,584	–177,834	667	65	Glacial marine mud	Open water AIO	
Mosola and Anderson, 2006	AA49689	Palmer	NBF99-02	TC	4	3–5	–26.2	5369	48	1706	–78,151	–168,58	618	34	Glacial marine mud	Open water AIO	
Mosola and Anderson, 2006	AA49690	Palmer	NBF99-02	TC	4	5–7	–24.8	8066	49	4403	–78,151	–168,58	618	34	Glacial marine mud	Open water AIO	
Mosola and Anderson, 2006	AA49691	Palmer	NBF99-02	TC	4	15–17	–24.1	18,160	140	14,497	–78,151	–168,58	618	34	Glacial marine mud	Open water AIO	
Mosola and Anderson, 2006	AA49692	Palmer	NBF99-02	TC	4	32–34	–24.9	23,950	230	20,287	–78,151	–168,58	618	34	Glacial marine mud	Open water AIO	
Mosola and Anderson, 2006	AA49693	Palmer	NBF99-02	PC	4	0–2	–25.2	21,160	140	17,497	–78,151	–168,58	618	104	Glacial marine mud	Open water AIO	
Mosola and Anderson, 2006	AA49694	Palmer	NBF99-02	PC	4	8–10	–24.9	23,950	230	20,287	–78,151	–168,58	618	104	Glacial marine mud	Open water AIO	
Mosola and Anderson, 2006	AA49695	Palmer	NBF99-02	PC	5	0–2	–26.8	3663	38	0	–77,251	–169,386	603	69	Glacial marine mud	Open water AIO	
Mosola and Anderson, 2006	AA49696	Palmer	NBF99-02	TC	5	11–13	–25.6	8967	62	5304	–77,251	–169,386	603	69	Glacial marine mud	Open water AIO	
Mosola and Anderson, 2006	AA49697	Palmer	NBF99-02	TC	5	66–68	–24.4	27,000	260	23,337	–77,251	–169,386	603	69	Glacial marine mud	Open water AIO	
Mosola and Anderson, 2006	AA49698	Palmer	NBF99-02	PC	5	5–7	–25.2	12,694	89	f	–77,251	–169,386	603	321	Glacial marine mud	Open water AIO	
Mosola and Anderson, 2006	AA49700	Palmer	NBF99-02	TC	6	11–13	–26.2	7421	57	3717	–77,251	–169,386	607	87	Glacial marine mud	Open water AIO	
Mosola and Anderson, 2006	AA49701	Palmer	NBF99-02	TC	6	36–38	–25.5	19,490	130	15,786	–77,251	–169,386	607	87	Glacial marine mud	Open water AIO	
Mosola and Anderson, 2006	AA49702	Palmer	NBF99-02	PC	6	4–6	–25.6	27,330	290	23,626	–77,251	–169,386	607	40	Glacial marine mud	Open water AIO	
Mosola and Anderson, 2006	AA49703	Palmer	NBF99-02	TC	7	0–2	–26.8	3704	39	0	–77,23	–169,419	580	70	Glacial marine mud	Open water AIO	
Mosola and Anderson, 2006	AA49704	Palmer	NBF99-02	TC	7	24–26	–25.5	13,325	67	9621	–77,23	–169,419	580	70	Glacial marine mud	Open water AIO	

Mosola and Anderson, 2006 AA49705	Palmer	NBP99-02	PC	7	0–2	–25.0	23,690	260	19,986	–77.23	–169,419	580	247	Glacial marine	Open water	
Mosola and Anderson, 2006 AA49706	Palmer	NBP99-02	KC	11	0–2	–25.6	4613	47	0	–76,311	–169,659	578	100	Glacial marine	Open water	AIO
Mosola and Anderson, 2006 AA49707	Palmer	NBP99-02	KC	11	5–7	–25.9	52,52	39	639	–76,311	–169,659	578	100	Glacial marine	Open water	AIO
Mosola and Anderson, 2006 AA49708	Palmer	NBP99-02	KC	11	9–11	–25.3	8247	46	3634	–76,311	–169,659	578	100	Glacial marine	Open water	AIO
Mosola and Anderson, 2006 AA49709	Palmer	NBP99-02	TC	13	4–6	–25.5	5948	39	1335	–76,205	–169,77	588	675	Glacial marine	Open water	AIO
Mosola and Anderson, 2006 AA49710	Palmer	NBP99-02	TC	13	16–18	–26.1	18,680	140	14,067	–76,205	–169,77	588	675	Glacial marine	Open water	AIO
Mosola and Anderson, 2006 AA49711	Palmer	NBP99-02	TC	13	22–24	–25.5	16,056	82	11,443	–76,205	–169,77	588	675	Glacial marine	Open water	AIO
Mosola and Anderson, 2006 AA49714	Palmer	NBP99-02	PC	13	28–30	–26.2	28,520	300	23,907	–76,205	–169,77	588	181	Glacial marine	Open water	AIO
Mosola and Anderson, 2006 AA49715	Palmer	NBP99-02	TC	14	0–2	–26.7	4013	37	0	–76,683	–166,135	443	25	Glacial marine	Open water	AIO
Mosola and Anderson, 2006 AA49713	Palmer	NBP99-02	TC	14	10–12	–26.5	5580	52	1567	–76,683	–166,135	443	25	Glacial marine	Open water	AIO
Mosola and Anderson, 2006 AA49716	Palmer	NBP99-02	TC	14	20–22	–25.9	6621	50	2608	–76,683	–166,135	443	25	Glacial marine	Open water	AIO
Mosola and Anderson, 2006 AA49717	Palmer	NBP99-02	PC	14	0–2	–26.5	5823	47	1810	–76,683	–166,135	443	68	Glacial marine	Open water	AIO
Mosola and Anderson, 2006 AA49717	Palmer	NBP99-02	TC	15	0–2	–27.0	4590	46	0	–76,374	–163,129	517	18	Glacial marine	Open water	AIO
Mosola and Anderson, 2006 AA49718	Palmer	NBP99-02	TC	15	12–14	–26.5	23,620	190	19,030	–76,374	–163,129	517	18	Glacial marine	Open water	AIO
Mosola and Anderson, 2006 AA49719	Palmer	NBP99-02	PC	15	4–6	–25.1	30,620	400	26,030	–76,374	–163,129	517	1825	Glacial marine	Open water	AIO
Mosola and Anderson, 2006 AA49720	Palmer	NBP99-02	TC	16	0–2	–26.1	4001	54	0	–76,995	–163,385	656	20	Glacial marine	Open water	AIO
Mosola and Anderson, 2006 AA49721	Palmer	NBP99-02	TC	16	17–19	–24.5	F	F	NA	–76,995	–163,385	656	20	Glacial marine	Open water	AIO
Mosola and Anderson, 2006 AA49722	Palmer	NBP99-02	PC	16	5–7	–25.7	F	F	NA	–76,995	–163,385	656	105	Glacial marine	Open water	AIO
Mosola and Anderson, 2006 AA49723	Palmer	NBP99-02	TC	17	0–2	–26.9	F	F	NA	–77.716	–161,862	715	58	Glacial marine	Open water	AIO
Mosola and Anderson, 2006 AA49724	Palmer	NBP99-02	PC	17	0–2	–26.5	F	F	NA	–77.716	–161,862	715	205	Glacial marine	Open water	AIO
Cunningham et al., 1999 AA17364	Palmer	NPB95-01	KC	31	0–2	2424	50	0	–75.7	165,417	879	210	Massive mud	Open water	AIO	
Cunningham et al., 1999 AA17365	Palmer	NPB95-01	KC	31	9–11	3140	50	715	–75.7	165,417	879	210	Massive mud	Open water	AIO	
Cunningham et al., 1999 AA17366	Palmer	NPB95-01	KC	31	49–51	5680	55	3255	–75.7	165,417	879	210	Massive mud	Open water	AIO	
Cunningham et al., 1999 AA17367	Palmer	NPB95-01	KC	31	116–118	10,230	70	7805	–75.7	165,417	879	210	Mud with sandy layers	Transitional	AIO	
Cunningham et al., 1999 AA17368	Palmer	NPB95-01	KC	31	159–161	12,275	95	9850	–75.7	165,417	879	210	Pebby, massive pebbly diamictic	Ice retreats past Drygalski	AIO	
Cunningham et al., 1999 AA20743	Palmer	NPB95-01	KC	31	167–169	–25.5	26,265	325	23,840	–75.7	165,417	879	210	Pebby, massive ice tongue	Glacial	AIO
Cunningham et al., 1999 AA20744	Palmer	NPB95-01	KC	31	200	–23.4	31,605	520	29,225	–75.7	165,417	879	210	Pebby, massive diamicton	Glacial	AIO
Cunningham et al., 1999 AA21766	Palmer	NPB95-01	KC	31	30–32	–25.9	3940	45	1515	–75.7	165,417	879	210	Massive mud	Open water	AIO
Cunningham et al., 1999 AA21767	Palmer	NPB95-01	KC	31	70–72	–25.4	5925	60	3500	–75.7	165,417	879	210	Massive mud	Open water	AIO
Cunningham et al., 1999 AA21768	Palmer	NPB95-01	KC	31	87–89	–25.5	7270	65	4845	–75.7	165,417	879	210	Massive mud	Open water	AIO
Cunningham et al., 1999 AA17357	Palmer	NPB95-01	KC	37	0–2	2775	50	0	–74,498	167,743	924	173	Massive mud	Open water	AIO	
Cunningham et al., 1999 AA17358	Palmer	NPB95-01	KC	37	20–21	4715	50	1940	–74,498	167,743	924	173	Ash-rich sand	Transitional	AIO	
Cunningham et al., 1999 AA17359	Palmer	NPB95-01	KC	37	40–41	8630	85	5855	–74,498	167,743	924	173	Massive mud	Transitional	AIO	
Cunningham et al., 1999 AA17360	Palmer	NPB95-01	KC	37	67–68	13,835	95	11,060	–74,498	167,743	924	173	Ash-rich sand	Transitional	AIO	
Cunningham et al., 1999 AA17361	Palmer	NPB95-01	KC	37	55–56	10,495	75	7720	–74,498	167,743	924	173	Massive mud	Open water	AIO	
Cunningham et al., 1999 AA17362	Palmer	NPB95-01	KC	37	30–31	6205	55	3430	–74,498	167,743	924	173	Massive mud	Open water	AIO	
Cunningham et al., 1999 AA17363	Palmer	NPB95-01	KC	37	10–11	3020	50	245	–74,498	167,743	924	173	Massive mud	Open water	AIO	
Cunningham et al., 1999 AA20747	Palmer	NPB95-01	KC	37	83–84	–25.2	17,800	175	15,025	–74,498	167,743	924	173	Massive mud	Transitional	AIO
Cunningham et al., 1999 AA20748	Palmer	NPB95-01	KC	37	146–148	–24.1	26,895	375	24,120	–74,498	167,743	924	173	Pebby, massive glacial	Glacial	AIO
Cunningham et al., 1999 AA21769	Palmer	NPB95-01	KC	37	125–127	–24.2	30,695	460	27,920	–74,498	167,743	924	173	Sandy mud	Transitional	AIO
Cunningham et al., 1999 AA23228	Palmer	NPB95-01	KC	37	93–95	–24.5	19,385	135	16,610	–74,498	167,743	924	173	Massive mud	Transitional	AIO

(continued on next page)

Table 1 (continued)

Reference	Lab no.	Ship	Cruise	Core type ^a	Core	Sample depth [cm]	$\delta^{13}\text{C}$	Age ^b yr BP	Error	Corrected age ^c yr BP	Latitude	Longitude	Water depth [mbsf]	Core length [cm]	Lithology	Interpretation	Type of carbon
Cunningham et al., 1999	AA17351	Palmer	NBP95-01	KC	39	0–1	3140	50	0	-74.473	173.512	557	257	Massive mud	Open water	AlO	
Cunningham et al., 1999	AA17352	Palmer	NPB95-01	KC	39	208–210	14290	95	11,150	-74.473	173.512	557	257	Sandy mud	Transitional	AlO	
Cunningham et al., 1999	AA17353	Palmer	NPB95-01	KC	39	100–101	7015	60	3875	-74.473	173.512	557	257	Massive mud	Open water	AlO	
Cunningham et al., 1999	AA17354	Palmer	NPB95-01	KC	39	190–191	10445	80	7305	-74.473	173.512	557	257	Massive mud	Open water	AlO	
Cunningham et al., 1999	AA17355	Palmer	NPB95-01	KC	39	50–51	4755	60	1615	-74.473	173.512	557	257	Massive mud	Open water	AlO	
Cunningham et al., 1999	AA17356	Palmer	NPB95-01	KC	39	150–151	7740	60	4600	-74.473	173.512	557	257	Massive mud	Open water	AlO	
Cunningham et al., 1999	AA19924	Palmer	NPB95-01	KC	39	230	-25.0	26,585	280	23,445	-74.473	173.512	557	257	Pebby, massive glacial diamicton	Glacial	AlO
Cunningham et al., 1999	AA19925	Palmer	NPB95-01	KC	39	249–250	-26.0	25,750	320	22,610	-74.473	173.512	557	257	diamicton	Pebby, massive glacial	AlO
Cunningham et al., 1999	AA21770	Palmer	NBP95-01	KC	39	80–82	-29.3	5820	90	2680	-74.473	173.512	557	257	Massive mud	Open water	AlO
Cunningham et al., 1999	AA21771	Palmer	NPB95-01	KC	39	170–172	-29.0	8980	70	5840	-74.473	173.512	557	257	Massive mud	Open water	AlO
Taviani et al., 1993 ^e		Glacier	DF87	PC	20	8–13		27,590	460	-72,538	174.97	622	85	Thick, gravelly calcareous sand	Barnacle/foraminifer facies	Not Reported	
Taviani et al., 1993 ^e		Glacier	DF87	PC	9	5–8		25,700	420	-73.14	174.97	622	85	Thick, gravelly calcareous sand	Barnacle/foraminifer facies	Not Reported	
Taviani et al., 1993 ^e		Glacier	DF87	PC	9	135–138		34,590		-73.14	177.113	548	220	Gravelly sandy mud, to muddy bryozoan/barnacle/pelecypod/foraminifer facies	Muddy bryozoan/barnacle/pelecypod/foraminifer facies	Not Reported	
Taviani et al., 1993 ^e		Eltanin	ELT52	PC	9	10–12		22,730	900	-72,447	173.872	479	220	Gravelly sandy mud, to muddy bryozoan/barnacle/pelecypod/foraminifer facies	Muddy bryozoan/barnacle/pelecypod/foraminifer facies	Not Reported	
Taviani et al., 1993 ^e		Glacier	DF87	PC	14	5–9		35,410		-72,973	-179.893	658	179	Clean, sorted to well sorted, foraminifer sands	Coarse bioclastic gravelly sands and muds	Not Reported	
Kellogg et al., 1990 ^d	QL-1126														interbedded with slightly muddy, gravelly, lithic sands.		
Kellogg et al., 1990 ^d	QL-1127														On BIDB near Barnacle north end	Barnacle	
Kellogg et al., 1990 ^d	QL-1128														On BIDB	Barnacle	
Kellogg et al., 1990 ^d	QL-1222														south of BIR		
Kellogg et al., 1990 ^d	QL-1129														North of Black Barnacle Island on BIDB		
Kellogg et al., 1990 ^d	QL-1132														Northeast of Scallop Hill	Barnacle	
Kellogg et al., 1990 ^d	QL-1223 ^f														Off east end of Minna Bluff		
Kellogg et al., 1990 ^d	QL-1130														On end of Scallop Hill	SHELLS	
Kellogg et al., 1990 ^d	QL-1131														Between Black Island and Brown Peninsula	Barnacle	

Kellogg et al., 1990 ^d	QL-1224	K76-64	4410	90	3395	-78.2250	165.6667	South of Dog Barnacle Leg
Kellogg et al., 1990 ^d	QL-1225	K76-66	1340	30	Modern	-77.8667	165.2500	Dailey Islands Bryozoa
Kellogg et al., 1990 ^d	QL-1226	K76-67A	3280	300	2034	-77.8917	165.0667	Dailey Islands Shells
Kellogg et al., 1990 ^d	QL-85	MT-2	4140	60	3074	-77.8917	165.8833	On northern Algae part of BIDB
Kellogg et al., 1990 ^d	QL-84	MT-2	5670	100	5090	-77.8917	165.8833	On northern Shells part of BIDB
Kellogg et al., 1990 ^d	QL-79	MT-3	1290	50	Modern	-78.1367	166.5167	Northeast Shells shore of Black Island
Kellogg et al., 1990 ^d	QL-167	MT-4	3130	90	1833	-78.2167	165.7000	South of Dog Shells Leg
Kellogg et al., 1990 ^d	QL-77	QL-97	1370	50	130.5	-77.9633	165.3000	Eastern Shells Dailey Islands, south side
Kellogg et al., 1990 ^d	QL-166	QL-166	3370	80	2104	-77.8750	165.3000	Eastern Shells Dailey Islands, east side
Kellogg et al., 1990 ^d	QL-1443	K78-15	6600	60	6096	-77.8000	165.6667	North end of Shells BIB (site no longer exists)
Kellogg et al., 1990 ^d	QL-1444	K78-18	7750	90	7361	-78.0417	165.8667	Swirls, Barnacle eastern edge
Kellogg et al., 1990 ^d	QL-1445	K78-20	2710	60	1368	-78.0000	165.6500	Swirls, Barnacle northern edge
Kellogg et al., 1990 ^d	QL-1446	K78-24	1890	60	586	-78.0000	165.6000	East of Barnacle Bratina Island
Kellogg et al., 1990 ^d	QL-1447	K78-67	45,500	1500	Radiocarbon dead	-77.9950	165.5333	On KGC, south end
Kellogg et al., 1990 ^d	QL-1448	K78-75	570	60	Modern	-78.1083	165.2500	Near north Bratina Island, on outlier
Kellogg et al., 1990 ^d	QL-1449	K78-78	4410	70	3398	-78.1583	165.8917	White Island, Barnacle Leg
Kellogg et al., 1990 ^d	QL-1450	K78-80	3190	50	1909	-78.1833	165.8333	Dog Leg, center
Kellogg et al., 1990 ^d	QL-1451	K78-100	5250	50	4523	-78.1967	165.7333	Dog Leg, south end
Kellogg et al., 1990 ^d	QL-4022	K78-104	35,400	1500	38,694	-78.0333	167.4000	White Island, Barnacle Speden [1962] site 19
Kellogg et al., 1990 ^d	QL-1452	K78-107	2530	50	1165	-78.4250	165.7500	North of Barnacle Minna Saddle Mount
Kellogg et al., 1990 ^d	QL-4023	K78-108	2150	40	801	-78.2717	165.7333	Discovery On KGC, south end
Kellogg et al., 1990 ^d	QL-1453	K78-110	720	60	Modern	-78.1500	165.1667	East of Brown Barnacle Peninsula saddle
Kellogg et al., 1990 ^d	QL-4023	K78-113	2160	50	810	-78.2167	165.5667	East of Brown Barnacle Peninsula saddle
Kellogg et al., 1990 ^d	QL-1454	K81-7	5610	50	5020	-78.2083	165.6000	On outlier, Barnacle northeast of Bratina Island
Kellogg et al., 1990 ^d	QL-4024	K81-14	3050	30	1732	-77.9833	165.5333	On outlier, Barnacle northwest of Bratina Island
Kellogg et al., 1990 ^d	QL-4025		30,900	160	34,179	-77.9883	165,5000	(continued on next page)

Table 1 (continued)

Reference	Lab no.	Ship	Cruise	Core type ^a	Core	Sample depth [cm]	$\delta^{13}\text{C}$	Age ^b yr BP	Error	Corrected age ^c cal yr BP	Latitude	Longitude	Water depth [mbsf]	Core length [cm]	Lithology	Interpretation	Type of carbon
Kellogg et al., 1990 ^d	QL-4026				K81-15			>46,000		5428	-77.9967	165.4833			Northwest of Bratina Island	Barnacle	
Kellogg et al., 1990 ^d	QL-4027				K81-17			22,070	140	24,753	-78.0083	165.5167			On Swirls, west of Bratina Island	Barnacle	
Kellogg et al., 1990 ^d	QL-4028				K81-18			20,760	80	23,131	-78.0117	165.5333			On Swirls, southwest of Bratina Island	Barnacle	
Kellogg et al., 1990 ^d	QL-4029				K81-21			4880	30	3999	-78.0200	165.5583			Con Swirls, south of Bratina Island	Barnacle	
Kellogg et al., 1990 ^d	QL-A030				K81-29			4430	30	3428	-78.1333	165.9917			West of north end of Black Island	Barnacle	
Kellogg et al., 1990 ^d	QL-4031				K81-33			2790	40	1452	-78.0917	166.0333			Northwest of Black Island	Barnacle	
Kellogg et al., 1990 ^d	QV4032				K81-39			4310	30	3263	-78.0917	165.9167			Northwest of Black Island	Barnacle	
Kellogg et al., 1990 ^d	QL-4033				K81-44			3820	30	2657	-78.2167	165.4833			On Swirls, near Brown Peninsula saddle	Barnacle	
Kellogg et al., 1990 ^d	QL-4034				K81-46			4900	30	4026	-78.2033	165.5000			On Swirls, near Brown Peninsula saddle	Barnacle	
Kellogg et al., 1990 ^d	QL-4035				K81-55			4150	30	3081	-78.4667	166.2833			North shore of Minna Bluff	Barnacle	
Kellogg et al., 1990 ^d				Fish				1100		Modern	-77.8833	165.2500			D. mawsoni near GOW-D1, Dailey Islands	Fish	
Kellogg et al., 1990 ^d				B&B				870	70	Modern	-78.1917	166.7333			On BIDB north of Scallop Hill	Algae	

Dates used for correction, by subtraction, from ages in corresponding core from Domack et al. (1999).

^a Core Type: PC- piston core, KC- Kasten core, TC- trigger core, HWD- hot water drill, G- grab sample.

^b All age corrections are based on original reference data. No additional corrections were made for this compilation.

^c Calibrations for Domack et al. (1999) calibrated by Livingstone et al. (2012).

^d All data from Kellogg et al. (1990) was calibrated using the standard 1300 year reservoir for the Ross Sea and the Marine 09 calibration curve from Calib6.0. Material dated: barnacle, Bathylasma corolliforme (Hoek); shells, mixed bryozoa, serpulids, barnacles, etc; algae, nonmarine algae from melt ponds; bryozoa, mixed bryozoan fragments; serpulids, serpulid worm tubes. Date on algae associated with mirabilite beds near K81-43 (Fig. 3).

^e All data from Taviani et al. (1993) are reported in Y.B.P.

^f Reported as QL-1123 in the work of Stuiver and Braziunas (1989).

^g Dates are uncorrected.

record the onset of open-marine conditions, which may lag grounding line retreat by thousands of years. In addition, these ages are fraught with uncertainties of reservoir correction (Reimer et al., 2009; Hall et al., 2010a) and reworking of old carbon from the sediment column (Andrews et al., 1999; Licht and Andrews, 2002; Ohkouchi and Eglinton, 2008; Rosenheim et al., 2008). It has been argued that diatomaceous facies contain a higher level of autochthonous organic material and that a correction for both of these complications can be achieved by subtracting core top AIO ages from down-core ages (Andrews et al., 1999; Domack et al., 1999). However, caution is needed because interpreting AIO ages relies on the assumption that the sedimentary environment has not changed significantly; specifically, that the input of old versus autochthonous organic matter has not changed through time. The most reliable results are considered to be those where multiple ages from a single diatom-rich unit lie in stratigraphic order with an age profile that is near-linear (e.g. Cunningham et al., 1999; Domack et al., 1999; McKay et al., 2008).

AIO ages from grounding-line proximal glacimarine sediments are considered even less reliable than diatomaceous glacimarine sediments due to reworking of old carbon, resulting in ages that are thousands of years older than the true age of deposition (Andrews et al., 1999). Indeed, it is common to find that glacimarine sediments appear to be significantly older than the overlying diatomaceous sediments (e.g. Cunningham et al., 1999; Domack et al., 1999; Mosola and Anderson, 2006; McKay et al., 2008). There are some carbonate ages that provide independent support for AIO ages (Table 1), but more carbonate dates are needed to help constrain the timing of ice-sheet retreat from the continental shelf. Despite the uncertainties, AIO ages have helped confirm that geomorphic features mapped on the Ross Sea floor were formed during the most recent advance(s) of the ice sheet onto the continental shelf, corroborating results from detailed high-resolution seismic stratigraphic investigations (Shipp et al., 1999; Mosola and Anderson, 2006; Bart and Cone, 2012).

Here we report both uncorrected (^{14}C ka BP) and corrected (cal ka BP) AIO ages only for cases where surface ages were provided by the original authors (Table 1). Where ages from carbonate material are reported, data were calibrated with a marine reservoir correction of 1.2–1.3 ka (Gordon and Harkness, 1992; Berkman and Forman, 1996; Andrews et al., 1999). Hall et al. (2010b) argue that this value is actually closer to 1.1 ka, similar to the estimate derived from fossil corals from McMurdo Sound and Terra Nova Bay. Table 1 lists values derived from the original sources.

Licht et al. (1996) argued that because cores from the outer shelf in western Ross Sea yielded AIO radiocarbon ages that were generally older than 20 cal ka BP, the ice sheet did not ground there during the LGM. Limited carbonate ages from the outer shelf support this interpretation (Anderson et al., 1992; Taviani et al., 1993). MSGL extend uninterrupted within Drygalski Trough to a location just north of Coulman Island where Shipp et al. (1999) placed the LGM grounding line (Fig. 6). This is approximately 50 km north of the LGM grounding line location picked by Licht et al. (1996).

Cunningham et al. (1999) obtained AIO radiocarbon chronologies and conducted detailed diatom assemblage analyses on two sediment cores located near the LGM grounding line location of Licht et al. (1996). Results from these studies indicate that the grounding line had shifted south of its Coulman Island location by ~13.0 cal ka BP. By ~11.0 cal ka BP, the grounding line was located in the vicinity of the present Drygalski Ice Tongue, suggesting an interval of slow retreat during that time interval (Licht et al., 1996, 1999; Cunningham et al., 1999; Domack et al., 1999; McKay et al., 2008). It then retreated rapidly to a location south of Ross Island ~7.8 cal ka BP (Licht et al., 1996; McKay et al., 2008). This grounding line location is in agreement with the ages of the oldest

shells and barnacles enclosed in the present-day McMurdo Ice Shelf by basal freeze on processes (Kellogg et al., 1990; Hall et al., 2010b), and with relative sea-level data indicating final unloading of grounded ice (Hall et al., 2004).

East of Mawson Bank, sediment cores from the outer shelf have yielded radiocarbon ages that indicate glacimarine sedimentation was occurring prior to the LGM (Frignani et al., 1998; Cunningham et al., 1999; Finocchiaro et al., 2000; Melis and Salvi, 2009), consistent with the outer shelf grounding-line location near Coulman Island (Fig. 6). AIO ages from diatomaceous sediments in Core NBP9501-39 (Fig. 4) are in stratigraphic order and indicate that marine conditions existed at this location by ~11.0 cal ka BP (Cunningham et al., 1999; Domack et al., 1999). Reliable radio-carbon ages needed to constrain grounding-line retreat across the inner shelf within JOIDES Basin are lacking.

Geomorphic features indicate that some of the ice coming from EAIS flowed between Pennell Bank and Ross Bank, exiting the Ross Sea through Pennell Trough (Fig. 6). Only a few radiocarbon ages have been acquired from cores within Pennell Trough and most of these sampled relatively young glacimarine sediments (Domack et al., 1999) or sediment gravity flow deposits (Salvi et al., 2006). One important exception is Core NBP94-01-PC31, which was collected near a field of recessional moraines that occur at the seaward bottleneck in the trough between Pennell Bank and Ross Bank (Shipp et al., 1999) (Fig. 4). This core yielded AIO radiocarbon ages from diatomaceous glacimarine sediments that are in stratigraphic order and extend back to at least ~13.3 cal ka BP (Domack et al., 1999), suggesting that grounding-line retreat from Pennell Trough was roughly coincident with that of the seaward JOIDES Trough and Drygalski Trough.

4.2. Evidence for asynchronous retreat

Mosola and Anderson (2006) acquired 39 AIO ages from sediment cores collected within Ross Sea troughs that lie to the east of the EAIS and WAIS paleodrainage confluence (Fig. 6). The ages of the oldest glacimarine sediments extend beyond LGM time. Mosola and Anderson (2006) argued that even with considerable reservoir correction (average surface age of ~4.0 cal ka BP) and ignoring the oldest ages in these cores, the data suggest retreat of the WAIS from the eastern continental shelf prior to retreat from the western Ross Sea and most likely during the LGM. Their argument was bolstered by three carbonate ages obtained by Licht and Andrews (2002) that, while out of stratigraphic order, indicate glacimarine sedimentation on the shelf began as early as ~22 cal ka BP. Licht and Andrews (2002) argued that these older ages came from foraminifera that had been reworked by re-advance of the ice sheet, but Mosola and Anderson (2006) argued that the re-working was more likely due to iceberg turbation, citing the abundance of iceberg furrows in the general area of the core site. Thus, these ages remain problematic in terms of their implications.

Utilizing a different strategy to date GZW deposition (as opposed to resumption of glacimarine sedimentation after ice-sheet retreat), Bart and Cone (2012) obtained radiocarbon ages from foraminifera isolated from sediments that were deposited on the foreset surface of a middle shelf GZW in the trough situated immediately east of the paleodrainage divide in central Ross Sea (Fig. 5c). Dating foraminifera deposited at the time of GZW formation should provide a direct age for a specific grounding line position. The GZW studied by Bart and Cone (2012) rests above a MSGL set that extends to the shelf margin and is overprinted by a younger MSGL set that terminates on the wedge (Fig. 5b). Thus, the wedge is assumed to have formed after the ice sheet extended to the shelf margin to form the older set of lineations. The combined ages from the wedge averaged 27.5 ^{14}C ka BP (~30.8 cal ka BP), suggesting retreat of the grounding

line from the outer shelf prior to this time and a grounding line pause sufficiently prolonged for GZW formation at 30.8 cal ka BP. Bart and Cone (2012) recognized the possibility of having reworked foraminifera in some of their samples, but their mixing model, which assumed up to 40% reworked foraminifera, predicted ages similar to the measured ages.

4.3. Timing of Holocene retreat inferred from land-based evidence

Terrestrial ages for retreat of ice from the northern Scott Coast come from relative sea level curves derived from ages of organic material in raised beaches (Baroni and Orombelli, 1991, 1994; Hall and Denton, 1999; Baroni and Hall, 2004; Hall et al., 2004). At Terra Nova Bay (Fig. 1), radiocarbon dates of shell, seal skin, and penguin remains bracket the age of the marine limit and the timing of complete unloading of grounded ice to ~8.2 cal ka BP (Baroni and Hall, 2004). This is somewhat later than the timing inferred from marine records, which indicate that the grounding line shifted to about this location after ~11.0 cal ka (Domack et al., 1999; Licht and Andrews, 2002; McKay et al., 2008). However, these ages are consistent with the presence of two lineages of geomorphic features, an older set of MSGL within the deeper part of Drygalski Trough that indicate flow to the north and a younger set of back-stepping GZW on the adjacent inner shelf that indicate flow toward the east and retreat to the west (Fig. 9). These latter features record the final phase of retreat from the shallower inner shelf, similar to what is observed farther south and north of Ross Island (Fig. 3b). There, along the southern Scott Coast, relative sea-level data indicate the grounding-line had retreated north of Ross Island by ~7.8 cal ka BP (Hall et al., 2004; Hall et al., 2013).

A large suite of ^{14}C dates derived from (i) algae within moraines deposited in ice-marginal ponds, as well as within glacioclustrine sediments from ice-dammed lakes, and (ii) shell, coral, and seal fragments in raised marine deposits help constrain the chronology around McMurdo Sound (Stuiver et al., 1981; Denton et al., 1989b; Denton and Marchant, 2000; Hall and Denton, 2000a, 2000b). The ages of LGM moraines at the mouth of Taylor Valley on Hjorth Hill range from ~18 to 13 cal ka BP (Hall and Denton, 2000a). New data from a similar moraine fronting the Royal Society Range confirm this age-range for the maximum ice extent (Allard et al., 2011; Koffman et al., 2011). The timing is also consistent with ^3He surface-exposure ages (~16–14 cal ka BP) from an equivalent moraine near Blue Glacier (Brook et al., 1995). Deltas that formed in proglacial lakes in Taylor Valley also attest to the presence of a grounded ice sheet in McMurdo Sound; the lakes could not have existed without grounded ice dams at the valley mouths. Ages from algae within deltas range from ~28.5 to 9.0 cal ka BP, indicating that a grounded ice sheet occupied McMurdo Sound throughout that time span (Stuiver et al., 1981; Clayton-Greene et al., 1988; Hall and Denton, 2000a, 2010a).

South of McMurdo Sound at the Darwin/Hatherton Glacier system, detailed analysis of soil development, along with ^{14}C ages of algae deposited in former ice-marginal ponds, indicate that the maximum ice thickness there was maintained until at least 13.0 cal ka BP, and present-day elevations were reached by 6.8 cal ka BP (Bockheim et al., 1989). Anderson et al. (2004) estimated the response time of the Hatherton/Darwin system to a perturbation to be ~1.1 ka; in this case the grounding line would have retreated past the mouth of Darwin Glacier ~7.9 cal ka BP. Farther south, ^{10}Be exposure ages of erratics along the margins of Reedy Glacier indicate that near the mouth at the Quartz Hills, the glacier was at a maximum from about 17.0 to 14.0 cal ka BP (Todd et al., 2010). Recently acquired data from Scott Glacier (Stone et al., 2009) are consistent with maximum glaciation at roughly the same time, followed by thinning throughout most of the Holocene.

In the eastern Ross Sea, ice-sheet thinning and the emergence of the nunataks in the coastal Ford Ranges of Marie Byrd Land started before ~11.0 cal ka BP and continued throughout the Holocene (Stone et al., 2003). This timing is supported by measurements of postglacial rebound of up to 7.2 ± 0.8 mm/yr in western Marie Byrd Land (Bevis et al., 2009); such high rates imply significant unloading of ice in the region during the mid-late Holocene (Ivins and James, 2005).

At Roosevelt Island in the eastern Ross Sea, the distinctive pattern of radar-detected stratigraphy beneath the divide has implications for the history of ice dynamics at the divide (Raymond, 1983). Matching the layer pattern with a time-dependent ice-flow model indicates that divide-flow started ~4–3 cal ka BP, and since that time the island has been thinning ~9 cm/yr (Conway et al., 1999; Martin et al., 2006). An important conclusion from these results is that the grounding line passed south of Roosevelt Island about 4–3 cal ka BP. Depth profiles of age and temperature from an ice core to the bed on the south summit of the island that was completed in December 2012 will be used to help constrain the glacial history in the eastern Ross Sea since the LGM (c.f. Price et al., 2007).

Emerging evidence suggests that the Siple Coast grounding-line position has been relatively stable for the past 2.0 cal ka. Analyses of flowstripes in the Ross Ice Shelf indicate that discharge through the TAM outlet glaciers has not changed significantly over the past 2.0 cal ka (Hulbe and Fahnestock, 2007). Exposure-age data from Cohen Nunataks near the mouth of Reedy Glacier just upstream from the present-day WAIS grounding line suggest that deglaciation there was complete 3.0–2.0 cal ka BP (Todd et al., 2010). Although the Ross Ice Streams exhibit significant short-term variability over century and millennial time scales (Conway et al., 2002; Hulbe and Fahnestock, 2007; Catania et al., 2012), overall, it appears that the system is now near steady state (Nereson and Raymond, 2001; Joughin and Tulaczyk, 2002; Hulbe and Fahnestock, 2004; Horgan and Anandakrishnan, 2006).

5. Discussion

Combined till provenance and marine geomorphic data provide a reasonably coherent picture of ice sheet paleodrainage in the Ross Embayment during the maximum extent of the ice sheet and suggests roughly equal contributions of ice flowing from east and west Antarctica (Fig. 6). Paleo-drainage in the western Ross Sea was strongly regulated by shelf physiography, with ice streams flowing through relatively narrow troughs bounded by prominent banks. The seaward portions of these banks remained free of grounded ice during the LGM, providing refugia for rather diverse benthic communities (Taviani et al., 1993). These banks also provided pinning points for the retreating ice sheet (Domack et al., 1999; Shipp et al., 1999; Howat and Domack, 2003; McKay et al., 2008) and may have developed into independent centers of ice flow similar to the present day Roosevelt Island. Indeed, the final stages of retreat are marked by grounding zone wedges and recessional moraines that indicate grounding line migration away from deep troughs and toward these banks (Shipp et al., 1999).

Combined onshore and offshore studies in the western Ross Embayment have provided constraints on the thickness of the ice sheet during the LGM. The LGM grounding line position in western Ross Sea is placed just north of Coulman Island, based on continuous MSGL that extend within Drygalski Trough to that location (Figs. 6, 9). Ice-sheet surface elevations along the coast north of Ross Island were generally less than 600 asl during the LGM. Within the northern portion of Drygalski Trough, the ice sheet had to be at least 1230 m thick in order to be grounded in the trough. South of Ross Island the ice sheet was thicker, reaching elevations between

900 m–1100 m asl near Hatherton Glacier and 1100 m–1200 m asl near Reedy and Scott Glaciers.

Fig. 10 provides ice sheet reconstructions for 15, 10 and 5 ka BP time slices. These reconstructions are based on the combined terrestrial and marine data. Ages from marine sediments suggest that the grounding line had retreated from its location north of Coulman Island by ~13 cal ka BP and within the trough was located in the vicinity of the Drygalski Ice Tongue ~11 cal ka BP. Terrestrial data indicate the ice sheet was still grounded in the vicinity of Terra Nova Bay ~8.2 cal ka BP, however, geomorphic data indicate different lineages of features suggesting that the younger ages record the final stage of retreat from the deep trough to the shallow inner shelf and Terra Nova Bay (Fig. 9).

The grounding line then retreated rapidly to a location north of Ross Island by 7.8 cal ka and south to Hatherton Glacier by ~6.8 cal ka. Farther south, exposure ages from nunataks near the

mouths of Scott and Reedy Glaciers indicate thinning during the mid to late Holocene, and the grounding line reached its present position around 2–3 cal ka BP. Marine geomorphic features from the southern Drygalski trough, north of Ross Island, indicate that the final phase of grounding line retreat toward the coast was marked by a reversal in flow direction from westward and northward to eastward as the grounding line retreated toward the coast (Fig. 3a,b).

The timing of retreat from the central Ross Sea remains unresolved. Today, ice streams from West Antarctica source this area. The simplest reconstruction is to assume that the grounding line started to retreat from the continental shelf more or less in step with the retreat from the western sector. An alternative hypothesis relies on the validity of radiocarbon ages from foraminifera in proximal glacimarine sediments (i.e. that there is no significant contamination by reworked foraminifera) associated with a mid-

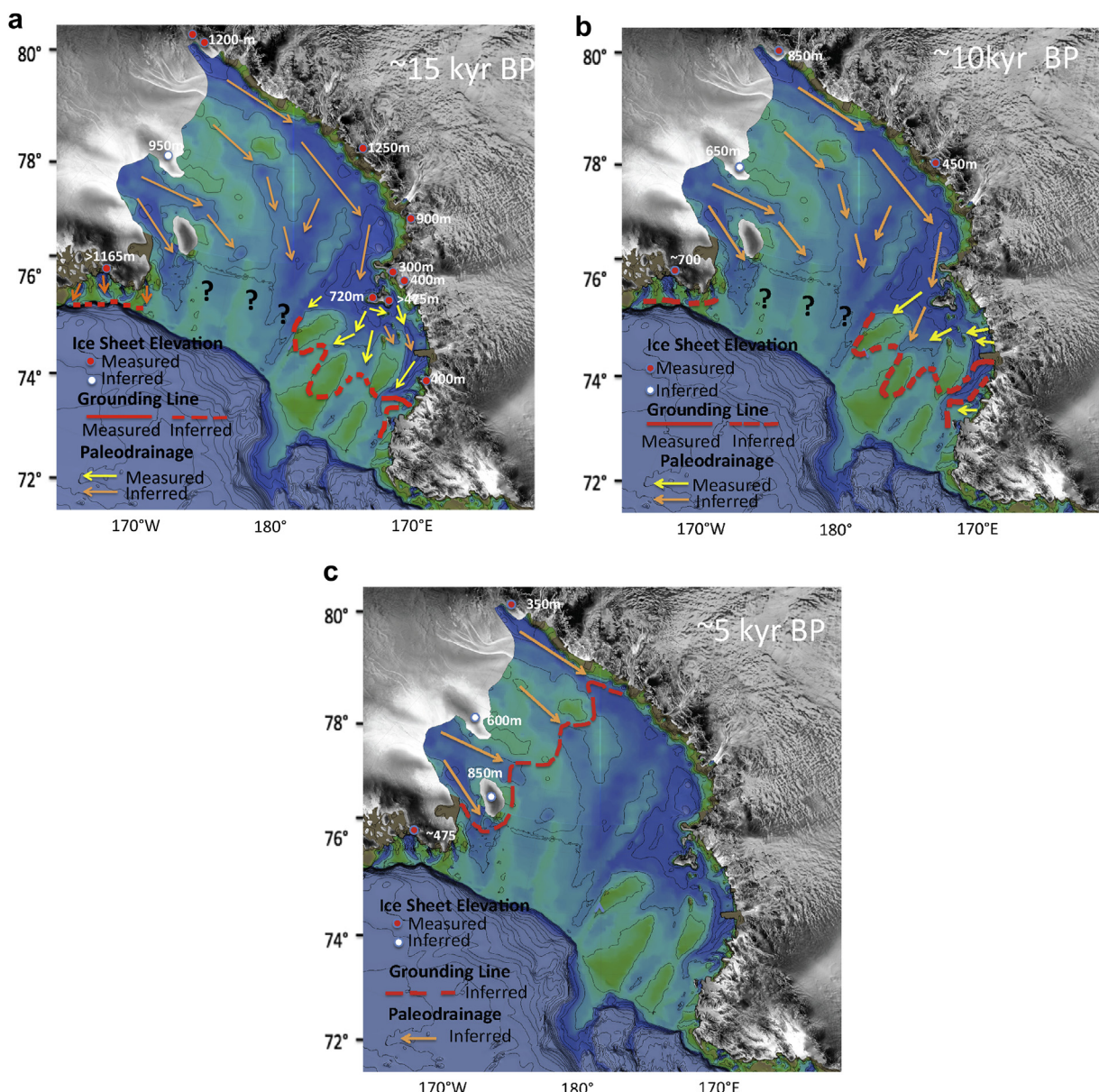


Fig. 10. Post-LGM ice sheet retreat history showing ice sheet elevations, grounding lines and paleoflow directions for 15, 10, and 5 ka BP. Terrestrial elevations along the range front (i.e. approximately along the current grounding line) are above present-day sea level and are not corrected for isostatic rebound. Red dot in the 15 ka reconstruction is location of sediment core NBP 94-31 and red dot in the 10 ka reconstruction is location of sediment core NBP 95-31.

shelf GZW (Bart and Cone, 2012). This wedge lies above MSGL that extend to the shelf margin and is overprinted by younger MSGL that terminate on the top of the wedge. The ages from the foraminifera indicate that grounded ice had retreated from the outer continental shelf by 27.5 ^{14}C ka BP (~ 30.8 cal ka BP) (Bart and Cone, 2012). These ages are generally consistent with early results from Mosola and Anderson (2006), although their older AIO ages are problematic. If the marine dates are correct, the implication is that the grounding line was well inland from the margin of the continental shelf in the central Ross Sea by LGM time and possibly even formed a deep embayment within the central Ross Sea. More reliable ages from marine sediments in the central Ross Embayment are needed to test and validate this hypothesis, but later retreat of the EAIS is supported by westward retreating GZW's in the western Ross Sea.

LGM elevations reconstructed from dated glacial limits in the mountains adjacent to the Ross Sea are nearly 150–200 m higher than those calculated from models constrained by radar-detected internal stratigraphy and the dated ice core from Siple Dome, located roughly equidistant between the Transantarctic Mountains and Marie Byrd Land (Fig. 1). The difference suggests that the central portion of the ice sheet fed by ice streams crossing the present-day Siple Coast was lower than the margins near the mountains, requiring streaming, low-gradient ice flow across the Ross Sea floor (Waddington et al., 2005; Ackert et al., 2007; Price et al., 2007). The argument that the ice streams were active during the LGM is also supported by the synchronicity between the onset of thinning far inland (i.e. Siple Dome and at Reedy Glacier) and the onset of grounding-line retreat from the outer continental shelf in the western Ross Sea by ~ 13.0 cal ka BP, resulting in an embayment in the grounding line within northern Drygalski Trough (Fig. 10b). The ice sheet had to be lightly grounded at that time in order to allow rapid transfer of longitudinal stress gradients over such large distances (Payne et al., 2004; Gudmundsson, 2007).

Although Siple Dome has been near steady state (constant thickness) for at least 10 ka (Nereson and Raymond, 2001; Price et al., 2007), Roosevelt Island has thinned about 300 m in the past 3 ka (Conway et al., 1999; Martin et al., 2006). That is, at ~ 3.0 cal ka BP the crest of Roosevelt Island was more than 800 m asl, while Siple Dome was only 600 m asl. This opens the possibility that a thick dome of ice existed over the Shirase Coast during the Holocene.

Subglacial geomorphic features extend to the shelf margin in Sulzberger Bay. Although there is a lack of radiometric constraints on the timing of ice sheet retreat from the continental shelf (Wellner et al., 2001), cosmogenic surface-exposure ages from the adjacent Ford Ranges indicate thick ice remained at the start of the Holocene (Stone et al., 2003), suggesting that most of the deglaciation occurred in the past 11 ka. The absence of reliable radiocarbon ages from the eastern continental shelf prevents us from testing this hypothesis further.

While the timing of ice sheet retreat in the central and eastern Ross Sea remains problematic, our reconstructions portray complex behavior of the ice sheets during their retreat from the continental shelf (Fig. 10). This complex behavior is not unexpected given the variable conditions that regulated ice sheet behavior during retreat, in particular the very different geology and physiographic settings of the two areas. Islands and banks in the western Ross Sea provided penning points that appear to have slowed the retreat of the ice sheet. In contrast, the central and eastern continental shelf is generally deeper and banks are absent. There, highly extended paleo-ice streams flowed more-or-less uninterrupted across the continental shelf within prominent cross-shelf troughs. These troughs are floored by unconsolidated Plio-Pleistocene sediments (Alonso et al., 1992) that contributed to a thick and extensive deforming bed (Shipp et al., 1999; Mosola and Anderson, 2006) This

configuration likely contributed to faster ice stream flow velocities and thinning of the ice sheet to the point where buoyancy forced decoupling from the sea floor soon after the ice sheet reached its outer shelf position and while the shelf was still isostatically depressed (Shipp et al., 1999; Howat and Domack, 2003; Mosola and Anderson, 2006).

6. Conclusions

Results from studies of till provenance and the orientations of geomorphic features on the Ross Sea continental shelf show that ice with East Antarctic origins extended across the continental shelf west of $\sim 180^\circ$. Thus, East Antarctic outlet glaciers supplied more than half the ice that filled the Ross Sea when the ice sheet was at its maximum configuration. This evidence precludes reconstructions in which an overwhelming flux of ice from West Antarctica confines flow from the outlet glaciers to a narrow corridor close to the western edge of the Ross Embayment (e.g. Stuiver et al., 1981). Moreover, available data indicate that the maximum ice elevation occurred later at inland sites than near the coast. Both of these observations support the idea that outlet-glacier thickening was a result of buttressing by grounded ice in the Ross Embayment during the LGM. The observed time-transgressive behavior between coastal and interior sites partly reflects the response time of interior sites to perturbations in the Ross Embayment, and it may also be a response to increased precipitation during the Holocene (Brook et al., 2005; Todd et al., 2010).

The main ambiguity in the glacial history of the Ross Embayment concerns central and eastern Ross Sea, where the ice from West Antarctica was discharging. There is compelling sedimentological and geomorphological evidence that the ice sheet advanced across the continental shelf to the shelf margin. It is the timing of ice sheet advance and retreat that is problematic. Two very different models for ice sheet retreat exist. One model relies on the validity of existing marine radiocarbon ages and calls for pre-LGM retreat of the ice sheet from the outer continental shelf. An alternate model calls for retreat of the ice sheet from the continental shelf that is generally synchronous with that of the western Ross Sea. Testing these models hinges on obtaining reliable radiocarbon ages from marine sediments, so this remains a high priority. But, the paucity of carbonate material is a major obstacle to achieving this objective. Recent advances in compound-specific radiocarbon age dating indicate that this method holds considerable promise for dating Antarctic marine sediments (Ohkouchi and Eglinton, 2008). The new ice core from Roosevelt Island will help constrain Holocene deglaciation in the eastern Ross Embayment.

In western Ross Sea, retreat of the ice sheet from the continental shelf occurred mainly after 13 cal yr BP and retreat was most rapid during the Holocene. Terrestrial data indicate that retreat in the central Ross Sea and eastern Ross Sea occurred at about the same time, but marine data indicate that retreat was much earlier. In either case, retreat of the ice sheet from the Ross Embayment occurred primarily after, and possibly before, MWP 1A. Thus, the Ross Embayment was not a significant contributor to the 10–15 m sea-level rise associated with that event, as argued by various authors (Clark et al., 2002, 2004; Weaver et al., 2003; Deschamps et al., 2012).

The development of high-resolution multibeam swath bathymetry systems has provided high-resolution images of geomorphic features formed during the retreat of the ice sheet that, in the past, could be obtained only in isolated areas using deep-tow, side-scan sonar. Those data that have been acquired provide evidence for episodes of rapid grounding line retreat and ice shelf collapse. Expanded surveys of these features will undoubtedly

provide opportunities to decipher a more detailed history of ice flow configuration and the spatial and temporal dynamics of ice streams during their retreat from the continental shelf.

It is not yet clear whether the present positive mass balance of the Ross Sea Sector (Rignot et al., 2008), and the apparent stability of the grounding-line position over the past 2 ka, is part of century-scale fluctuations of the ice streams, or whether it represents a reversal of the long-term Holocene retreat of the ice sheet (Conway et al., 1999; Hall et al., 2013).

Acknowledgments

We thank all of the many colleagues and students, past and present, who have worked with us on the glacial history of the Ross Sea region. The Office of Polar Programs of the National Science Foundation funded the US component of this work. The Swedish component was funded by the Swedish Polar Research Secretariat, Swedish Research Council and the New Zealand component by the New Zealand Foundation for Research Science and Technology.

References

- Ackert, R., et al., 1999. Measurement of past ice sheet elevations in interior West Antarctica. *Science* 286, 276–280.
- Ackert, R., Mukhopadhyay, S., Parizek, B., Borns Jr., H.W., 2007. Ice elevation near the West Antarctic Ice Sheet divide during the last glaciation. *Geophys. Res. Lett.* 34, L21506. <http://dx.doi.org/10.1029/2007GL031412>.
- Ackert, R., Mukhopadhyay, S., Pollard, D., DeConto, R.M., Putnam, A.E., Borns, H.W., 2011. West Antarctic Ice Sheet elevations in the Ohio Range: geologic constraints and ice sheet modeling prior to the last highstand. *Earth Planet. Sci. Lett.* 307, 83–93.
- Allard, S., Hall, B.L., Denton, G.H., 2011. History of the Ross Sea ice sheet based on glacial and lake records from Marshall Valley, Antarctica. In: 18th Annual West Antarctic Ice Sheet Meeting, Loveland, CO.
- Alley, R.B., Blankenship, D.D., Bentley, C.R., Rooney, S.T., 1986. Deformation of till beneath ice stream B, West Antarctica. *Nature* 322, 57–59.
- Alonso, B., Anderson, J.B., Diaz, J.T., Bartek, L.R., 1992. Pliocene-Pleistocene seismic stratigraphy of the Ross Sea: evidence for multiple ice sheet grounding episodes. In: Elliot, D.H. (Ed.), Contributions to Antarctic Research III, Antarctic Research Series, vol. 57. American Geophysical Union, Washington, D.C, pp. 93–103.
- Anderson, B., Hindmarsh, R.C., Lawson, W., 2004. A modelling study of the response of Hatherton Glacier to Ross Ice Sheet grounding line retreat. *Glob. Planet. Chang.* 42, 143–153.
- Anderson, J.B., Kurtz, D.D., Domack, E.W., Balshaw, K.M., 1980. Antarctic glacial marine sediments. *J. Geol.* 88, 399–414.
- Anderson, J.B., Brake, C.F., Myers, N.C., 1983. Sedimentation in the Ross Sea, Antarctica. *Mar. Geol.* 57, 295–333.
- Anderson, J., Shipp, S., Bartek, L., Reid, D.E., 1992. Evidence for a grounded ice sheet on the Ross Sea continental shelf during the late Pleistocene and preliminary paleodrainage reconstruction. *Am. Geophys. Union Antarct. Res. Ser.* 57, 39–62.
- Anderson, J.B., Shipp, S.S., Lowe, A.L., Wellner, J.S., Mosala, A.B., 2002. The Antarctic ice sheet during the last glacial maximum and its subsequent retreat history: a review. *Quat. Sci. Rev.* 21, 49–70.
- Andrews, J.T., Domack, E.W., Cunningham, W.L., Leventer, A., Licht, K.J., Jull, A.J.T., DeMaster, D.J., Jennings, A.E., 1999. Problems and possible solutions concerning radiocarbon of surface marine sediments, Ross Sea, Antarctica. *Quat. Sci. Rev.* 52, 206–216.
- Baroni, C., Hall, B.L., 2004. A new Holocene relative sea-level curve for Terra Nova Bay, Victoria Land, Antarctica. *J. Quat. Sci.* 19, 377–396.
- Baroni, C., Orombelli, G., 1991. Holocene raised beaches at Terra Nova Bay, Victoria Land, Antarctica. *Quat. Res.* 36, 157–177.
- Bart, P.J., Cone, A.N., 2012. Early stall of West Antarctic Ice Sheet advance on the eastern Ross Sea middle shelf followed by retreat at 27,500 ^{14}C yr BP. *Palaeogeogr. Palaeoclimatol. Palaeoecol.* 335–336, 52–60.
- Bart, P.J., Owolana, B., 2012. On the duration of West Antarctic Ice Sheet grounding events in Ross Sea during the Quaternary. *Quat. Sci. Rev.* 47, 101–115.
- Bartek, L.R., Anderson, J.B., 1991. Facies distribution resulting from sedimentation under polar interglacial climatic conditions within a high-latitude marginal basin, McMurdo Sound, Antarctica. In: Anderson, J.B., Ashley, G.M. (Eds.), Palaeoclimatic Interpretation of Glacial Marine Deposits, Special Publication 261, Geological Society of America, Boulder, CO, pp. 27–49.
- Berkman, P.A., Forman, S.L., 1996. Pre-bomb radiocarbon and the reservoir correction for calcareous marine species in the Southern Ocean. *Geophys. Res. Lett.* 23, 363–366.
- Bevis, M., et al., 2009. Geodetic measurements of vertical crustal velocity in West Antarctica and the implications for ice mass balance. *Geochem. Geophys. Geosyst.* 10, Q10005. <http://dx.doi.org/10.1029/2009GC002642>.
- Bockheim, J., Wilson, S.C., Denton, G.H., Andersen, B.G., Stuiver, M., 1989. Late Quaternary ice-surface fluctuations of Hatherton Glacier, Transantarctic Mountains. *Quat. Sci. Rev.* 31, 229–254.
- Brambati, A., Corradi, N., Finocchiaro, F., Giglio, F., 2002. The position of the Last Glacial Maximum grounding line in the Joides Basin: an interpretation based on sedimentological and geotechnical data. *Bull. R. Soc. N. Z.* 35, 365–372.
- Bromley, G.R., Hall, B.L., Stone, J.O., Conway, H., Todd, C., 2010. Late Cenozoic deposits at Reedy Glacier, Transantarctic Mountains: implications for former thickness of the West Antarctic Ice Sheet. *Quat. Sci. Rev.* 29, 384–398.
- Bromley, G.R., Hall, B.L., Stone, J.O., Conway, H., Todd, C., 2012. Late Cenozoic deposits at Scott Glacier, Transantarctic Mountains: implications for former thickness of the West Antarctic Ice Sheet. *Quat. Sci. Rev.* 50, 1–13.
- Brook, E., Kurz, M., Ackert, R., Raisbeck, G.M., Yiou, F., 1995. Comogenic nuclide exposure ages and glacial history of late Quaternary Ross Sea drift in McMurdo Sound, Antarctica. *Earth Planet. Sci. Lett.* 131, 41–56.
- Brook, E., White, J., Schilla, A., Bender, M., Barnett, B., Severinghaus, J., Taylor, K., Alley, R., Steig, E., 2005. Timing of millennial-scale climate change at Siple Dome, West Antarctica during the last glacial period. *Quat. Sci. Rev.* 24, 1333–1343.
- Casassa, G., Jezek, K.C., Turner, J., Whillans, I.M., 1991. Relict flowstripes on the Ross Ice Shelf. *Ann. Glaciol.* 15, 132–138.
- Catania, G., Hulbe, C., Conway, H., Scambos, T.A., Raymond, C.F., 2012. Variability in the mass flux of the Ross Sea ice streams, Antarctica, over the last millennium. *J. Glaciol.* 58 (210), 741–752. [http://dx.doi.org/10.3189/2012JoG11\[219](http://dx.doi.org/10.3189/2012JoG11[219).
- Clark, P.U., Dyke, A.S., Shakun, J.D., Carlson, A.E., Clark, J., Wohlfarth, B., Mitrovica, J.X., Hostettler, S.W., McCabe, A.M., 2009. The Last Glacial Maximum. *Science* 325 (5941), 710–714.
- Clark, P.U., Mitrovica, J.X., Milne, G.A., Tamisiea, M.E., 2002. Sea-level finger printing as a direct test for the source of global Meltwater Pulse 1A. *Science* 295, 2438–2441.
- Clark, P.U., McCabe, A.M., Mix, A.C., Weaver, A.J., 2004. Rapid rise of sea level 19,000 years ago and its global implications. *Science* 304, 1141–1144.
- Clayton-Greene, J., Hendy, C., Hogg, A., 1988. Chronology of a Wisconsin age pro-glacial lake in the Miers Valley, Antarctica. *N. Z. J. Geol. Geophys.* 31, 353–361.
- Conway, H., Hall, B.L., Denton, G.H., Gades, A.M., Waddington, E.D., 1999. Past and future grounding-line retreat of the West Antarctic Ice Sheet. *Science* 286, 280–283.
- Conway, H., Catania, G., Raymond, C.F., Gades, A.M., Scambos, T.A., Engelhardt, H., 2002. Switch of flow direction in an Antarctic ice stream. *Nature* 419, 465–467.
- Cunningham, W.L., Leventer, A., Andrews, J.T., Jennings, A.E., Licht, K.J., 1999. Late Pleistocene–Holocene marine conditions in the Ross Sea, Antarctica: evidence from the diatom record. *Holocene* 9, 129–139.
- Dagel, M., 1985. Stratigraphy and Chronology of Stage 6 and Stage 2 Glacial Deposits in Marshall Valley, Antarctica (M.S. thesis). University of Maine, Orono, Maine.
- David, T.W.E., Priestley, G.E., 1914. Glaciology, Physiography, Stratigraphy, and Tectonic Geology of South Victoria Land. British Antarctic Expedition, 1907–1909, Reports of the Scientific Investigations, Geology.
- Denton, G.H., Hughes, T., 2000. Reconstruction of the Ross ice drainage system, Antarctica, at the last glacial maximum. *Geogr. Ann.* 82A, 143–166.
- Denton, G.H., Marchant, D., 2000. The geologic basis for a reconstruction of a grounded ice sheet in McMurdo Sound, Antarctica, at the last glacial maximum. *Geogr. Ann.* 82A, 167–212.
- Denton, G.H., Bockheim, J., Wilson, S., Leide, J., Andersen, B.G., 1989a. Late Quaternary ice-surface fluctuations of Beardmore Glacier, Transantarctic Mountains. *Quat. Res.* 31, 183–209.
- Denton, G.H., Bockheim, J., Wilson, S., Stuiver, M., 1989b. Late Wisconsin and early Holocene glacial history, inner Ross Embayment, Antarctica. *Quat. Res.* 31, 151–182.
- Deschamps, P., Durand, N., Bard, E., Hamelin, B., Camoin, G., Thomas, A.L., Henderson, G.M., Okuno, J., Yokoyama, Y., 2012. Ice-sheet collapse and sea-level rise at the Bølling warming 14,600 years ago. *Nature* 483, 559–564.
- Dochat, T.M., Marchant, D., Denton, G.H., 2000. Glacial geology of Cape Bird, Ross Island, Antarctica. *Geogr. Ann.* 82A, 237–247.
- Domack, E., Jacobson, E., Shipp, S., Anderson, J., 1999. Late Pleistocene-Holocene retreat of the West Antarctic Ice Sheet in the Ross Sea: part 2-sedimentologic and stratigraphic signature. *Geol. Soc. Am. Bull.* 111, 1517–1536.
- Dowdeswell, J.A., Otteson, D., Evans, J., O'Cofaigh, C.O., Anderson, J.B., 2008. Submarine glacial landforms and rates of ice-stream collapse. *Geology* 36, 819–822.
- Dunbar, R., Anderson, J.B., Domack, E.W., Jacobs, S.S., 1985. Oceanographic influences on sedimentation along the Antarctic continental shelf: oceanology of the Antarctic Continental Shelf. *Am. Geophys. Union Antarct. Res. Ser.* 43, 291–312.
- Fahnstock, M., Scambos, T., Bindschadler, R., Kvaran, G., 2000. A millennium of variable ice flow recorded by the Ross Ice Shelf, Antarctica. *J. Glaciol.* 46 (155), 652–664.
- Farmer, G.L., Licht, K., Swope, R.J., Andrews, J.T., 2006. Isotopic constraints on the provenance of fine-grained sediment in LGM tills from the Ross Embayment, Antarctica. *Earth Planet. Sci. Lett.* 249, 90–107.
- Finocchiaro, F., Melis, R., Tosato, M., 2000. Late Quaternary environmental events in two cores from Southern Joides Basin (Ross Sea, Antarctica). In: Proceedings Workshop Palaeoclimatic Reconstructions from Marine Sediments of the Ross Sea (Antarctica) and Southern Ocean, vol. 4. Terra Antarctica Report, Trieste, Italy, pp. 125–130.

- Fagnani, M., Giglio, F., Langone, L., Ravaioli, M., Mangini, A., 1998. Late Pleistocene–Holocene sedimentary fluxes of organic carbon and biogenic silica in the north-western Ross Sea, Antarctica. *Ann. Glaciol.* 27, 697–703.
- Gordon, J.E., Harkness, D.D., 1992. Magnitude and geographic variation of the radiocarbon content in Antarctic marine life: implications for reservoir corrections in radiocarbon dating. *Quat. Sci. Rev.* 11, 696–708.
- Greenwood, S.L., Gyllencreutz, R., Jakobsson, M., Anderson, J.B., 2012. Ice flow switching and East/West Antarctic Ice Sheet roles in glaciation of the western Ross Sea. *Geol. Soc. Am. Bull.* <http://dx.doi.org/10.1130/B30643.1>.
- Gudmundsson, G.H., 2007. Tides and the flow of Rutford Ice Stream, West Antarctica. *J. Geophys. Res.* 112 (F4), F04007. <http://dx.doi.org/10.1029/2006F000731>.
- Hall, B.L., Denton, G.H., 1999. New relative sea-level curves for the southern Scott Coast, Antarctica: evidence for Holocene deglaciation of the western Ross Sea. *J. Quat. Sci.* 14, 641–650.
- Hall, B.L., Denton, G.H., 2000a. Radiocarbon chronology of Ross Sea drift, eastern Taylor Valley, Antarctica: evidence for a grounded ice sheet in the Ross Sea at the last glacial maximum. *Geogr. Ann.* 82A, 305–336.
- Hall, B.L., Denton, G.H., 2000b. Extent and chronology of the Ross Sea ice sheet and the Wilson Piedmont Glacier along the Scott Coast at and since the last glacial maximum. *Geogr. Ann.* 82A, 275–303.
- Hall, B.L., Denton, G.H., Hendy, C., 2000. Evidence from Taylor Valley for a grounded ice sheet in the Ross Sea, Antarctica. *Geogr. Ann.* 82A, 275–304.
- Hall, B.L., Denton, G.H., Baroni, C., 2004. Holocene relative sea-level history of the Southern Victoria Land Coast, Antarctica. *Glob. Planet. Chang.* 42, 241–263.
- Hall, B.L., Denton, G.H., Fountain, A.G., Hendy, C., Henderson, G., 2010a. Antarctic lakes suggest millennial reorganizations of Southern Hemisphere atmospheric and oceanic circulation. *Proc. Natl. Acad. Sci.* 107, 21355–21359.
- Hall, B.L., Henderson, G., Baroni, C., Kellogg, T., 2010b. Constant Holocene southern-ocean ^{14}C reservoir ages and ice-shelf flow rates. *Earth Planet. Sci. Lett.* 296, 115–123.
- Hall, B.L., Denton, G.H., Stone, J.O., Conway, H., 2013. History of the grounded ice sheet in the Ross Sea sector of Antarctica during the Last Glacial Maximum and the Last Termination. In: Geological Society of London, Special Publication, vol. 381. <http://dx.doi.org/10.1144/SP381.5>.
- Horgan, H.J., Anandakrishnan, S., 2006. Static grounding lines and dynamic ice streams: evidence from the Siple Coast, West Antarctica. *Geophys. Res. Lett.* 33. <http://dx.doi.org/10.1029/2006GL027091>.
- Howat, I.M., Domack, E.W., 2003. Reconstructions of western Ross Sea palaeo-ice-stream grounding zones from high-resolution acoustic stratigraphy. *Boreas* 32, 56–75.
- Hughes, T., 1973. Is the West Antarctic Ice Sheet disintegrating? *J. Geophys. Res.* 78, 7884–7910.
- Hulbe, C., Fahnestock, M., 2004. West Antarctic ice-stream discharge variability: mechanism, controls and pattern of grounding-line retreat. *J. Glaciol.* 50, 471–484.
- Hulbe, C., Fahnestock, M., 2007. Century-scale discharge stagnation and reactivation of Ross ice streams, West Antarctica. *J. Geophys. Res. Earth* 112, F03S27.
- Ivins, E.R., James, T.S., 2005. Antarctic glacial isostatic adjustment: a new assessment. *Antarct. Sci.* 17 (4), 537–549.
- Jakobsson, M., Anderson, J.B., Nitsche, F., Dowdeswell, J.A., Gyllencreutz, R., Kirchner, N., Mohammad, R., O'Regan, M., Alley, R.B., Anandakrishnan, S., Eriksson, B., Kirchner, A., Fernandez, R., Stolldorf, T., Minzoni, R., Majewski, W., 2011. Geological record of ice shelf break-up and grounding line retreat, Pine Island Bay, West Antarctica. *Geology* 39, 691–694.
- Joughin, I., Tulaczyk, S., 2002. Positive mass balance of the Ross Ice Streams, West Antarctica. *Science* 295, 476–480.
- Kellogg, T.B., Truesdale, R.S., Osterman, L.E., 1979. Late Quaternary extent of the West Antarctic Ice Sheet: new evidence from the Ross Sea cores. *Geology* 7, 249–253.
- Kellogg, T.B., Kellogg, D., Stuiver, M., 1990. Late Quaternary history of the south-western Ross Sea: evidence from debris bands on the McMurdo Ice Shelf. *Am. Geophys. Union Antarct. Res. Ser.* 50, 25–56.
- Koffman, T., Hall, B.L., Denton, G.H., 2011. New radiocarbon dates from glacial deposits in Miers Valley constrain the past behavior of the Antarctic Ice Sheet. In: 18th Annual West Antarctic Ice Sheet Meeting, Loveland, CO.
- Licht, K., Jennings, A.E., Andrews, J.T., Williams, K., 1996. Chronology of late Wisconsin ice retreat from the western Ross Sea, Antarctica. *Geology* 24, 223–226.
- Licht, K., Dunbar, N., Andrews, J.T., Jennings, A.E., 1999. Distinguishing subglacial till and glacial marine diamictites in the western Ross Sea, Antarctica: implications for a last glacial maximum grounding line. *Geol. Soc. Am. Bull.* 111, 91–103.
- Licht, K., Andrews, J.T., 2002. A ^{14}C record of late Pleistocene ice advance and retreat in the central Ross Sea, Antarctica. *Arct. Alp. Res.* 34, 324–333.
- Licht, K., Lederer, J.R., Swope, R.J., 2005. Provenance of LGM glacial till (sand fraction) across the Ross Embayment, Antarctica. *Quat. Sci. Rev.* 24, 1499–1520.
- Licht, K., Lederer, J., Farmer, G.L., Swope, R.J., Andrews, J.T., 2006. Petrographic and isotopic composition of Late Quaternary Ross Embayment till. *Terra Antarct. Rep.* 12, 35–42.
- Licht, K., Palmer, E.F., 2013. Glacial erosion and transport by Byrd Glacier, Antarctica during the Last Glacial Maximum. *Quat. Sci. Rev.* 62, 32–48.
- Livingstone, S.J., Ó Cofaigh, C., Stokes, C.R., Hillenbrand, C.-D., Vieli, A., Jamieson, S.S.R., 2012. Antarctic palaeo-ice streams. *Earth-Sci. Rev.* 111, 90–128.
- Martin, C., Hindmarsh, R.C., Navarro, F., 2006. Dating ice flow change near the flow divide at Roosevelt Island using a thermomechanical model to predict radar stratigraphy. *J. Geophys. Res.* 111. <http://dx.doi.org/10.1029/2005F00026>.
- McKay, R.M., Dunbar, G.B., Naish, T.R., Barrett, P.J., Carter, L., Harper, M., 2008. Retreat history of the Ross Ice Sheet (Shelf) since the Last Glacial Maximum from deep-basin sediment cores around Ross Island. *Palaeogeogr. Palaeoclimatol. Palaeoecol.* 260, 245–261.
- Melis, R., Salvi, G., 2009. Late Quaternary foraminiferal assemblages from western Ross Sea (Antarctica) in relation to the main glacial and marine lithofacies. *Mar. Micropaleontol.* 70, 39–53.
- Mercer, J.H., 1968. Antarctic Ice and Sangamon Sea Level. In: International Association of Scientific Hydrology Symposia, vol. 79, pp. 217–225.
- Merry, C.J., Whillans, I., 1993. Ice-flow features on Ice Stream B, Antarctica, revealed by SPOT HRV imagery. *J. Glaciol.* 39 (133), 515–527.
- Mosola, A.B., Anderson, J.B., 2006. Expansion and rapid retreat of the West Antarctic Ice Sheet in Eastern Ross Sea: possible consequence of over extended ice streams? *Quat. Sci. Rev.* 25, 2177–2196.
- Nereson, N.A., Raymond, C.F., 2001. The elevation history of ice streams and the spatial accumulation pattern along the Siple Coast of West Antarctica, inferred from ground-based radar data from three inter-stream ridges. *J. Glaciol.* 47 (157), 303–313.
- Ohkouchi, N., Eglington, T.I., 2008. Compound-specific radiocarbon dating of Ross Sea sediments: a prospect for constructing chronologies in high-latitude oceanic sediments. *Quat. Geochron.* 3, 235–243.
- Orombelli, G., Baroni, C., Denton, G.H., 1990. Late Cenozoic glacial history of the Terra Nova Bay region, Northern Victoria Land, Antarctica. *Geogr. Fis. Din. Quat.* 13, 139–163.
- Parizek, B.R., Alley, R.B., 2004. Ice thickness and isostatic imbalances in the Ross Embayment, West Antarctica: model results. *Glob. Planet. Chang.* 42, 265–278.
- Parizek, B.R., Alley, R.B., Hulbe, C.L., 2003. Subglacial thermal balance permits ongoing grounding line retreat along the Siple Coast of West Antarctica. *Ann. Glaciol.* 36, 251–256.
- Payne, A.J., Vieli, A., Shepherd, A.P., Wingham, D.J., Rignot, E., 2004. Recent dramatic thinning of largest West Antarctic ice stream triggered by oceans. *Geophys. Res. Lett.* 31, L23401. <http://dx.doi.org/10.1029/2004GL021284>.
- Péwé, T., 1960. Multiple glaciations in the McMurdo Sound region, Antarctica – a progress report. *J. Geol.* 68, 498–514.
- Price, S.F., Conway, H., Waddington, E.D., 2007. Evidence for late Pleistocene thinning of Siple Dome, West Antarctica. *J. Geophys. Res.* 112. <http://dx.doi.org/10.1029/2006F000725> (F03021).
- Raymond, C.F., 1983. Deformation in the vicinity of ice divides. *J. Glaciol.* 29, 357–373.
- Reimer, P.J., et al., 2009. INTCAL09 and Marine09 radiocarbon age calibration curves, 0–50,000 years cal BP. *Radiocarbon* 51, 1111–1150.
- Rignot, E., Bamber, J.L., van den Broeke, M.R., Davis, C., Li, Y., van de Berg, W.J., Meijgaard, E.V., 2008. Recent Antarctic ice mass loss from radar interferometry and regional climate modeling. *Nat. Geosci.* 1, 106–110.
- Rosenheim, B.E., Day, M.B., Schrum, H., Domack, E.W., Benthiem, A., Hayes, J.M., 2008. Antarctic sediment chronology by programmed temperature pyrolysis: methodology and data treatment. *Geochem. Geophys. Geosyst.* 9, Q04005. <http://dx.doi.org/10.1029/2007GC001816>.
- Salvi, C., Busetto, M., Marinoni, L., Brambati, A., 2006. Late Quaternary glacial marine to marine sedimentation in the Pennell Trough (Ross Sea, Antarctica). *Palaeogeogr. Palaeoclimatol. Palaeoecol.* 231, 199–214.
- Scott, R.F., 1905. The Voyage of the Discovery, vol. 2. Macmillan and Company, London, p. 260.
- Shabtaie, S., Bentley, C.R., 1982. Tabular icebergs: implications from geophysical studies of ice shelves. *J. Glaciol.* 28 (100), 413–430.
- Shipp, S., Anderson, J., Domack, E., 1999. Late Pleistocene-Holocene retreat of the West Antarctic Ice Sheet system in the Ross Sea: part 1-geophysical results. *Geol. Soc. Am. Bull.* 111, 1486–1516.
- Shipp, S.S., Wellner, J.S., Anderson, J.B., 2002. Retreat significance of a polar ice stream: sub-glacial geomorphic features and sediments from the Ross Sea, Antarctica. In: Dowdeswell, J.A., O'Cofaigh, C. (Eds.), *Glacier-influenced Sedimentation on High Latitude Continental Margins*, Geological Society of London, Special Publication, vol. 203, pp. 277–304. London, U.K.
- Stone, J.O., et al., 2003. Holocene deglaciation of Marie Byrd Land, West Antarctica. *Science* 299, 99–102.
- Stone, J.O., Conway, H., Cowdery, S., Hall, B.L., Bromley, G.R., 2009. Deglaciation of the Ross Sea: the view from Scott and Beardmore Glaciers. In: 16th Annual West Antarctic Ice Sheet Meeting, Eatontown, Washington.
- Stuiver, M., Denton, G.H., Hughes, T., Fastook, J., 1981. History of the Marine Ice Sheet in West Antarctica during the last glaciation. In: Denton, G., Hughes, T. (Eds.), *The Last Great Ice Sheets*. Wiley Interscience, New York, pp. 319–436.
- Stuiver, M., Braziunas, T.F., 1989. Atmospheric ^{14}C and century-scale solar oscillations. *Nature* 338, 405–408.
- Taviani, M., Reid, D.E., Anderson, J.B., 1993. Skeletal and isotopic composition and paleoclimatic significance of Late Pleistocene carbonates, Ross Sea, Antarctica. *J. Sediment. Res.* 63 (1), 84–90.
- Todd, C., Stone, J.O., Conway, H., Hall, B.L., Bromley, G.R., 2010. Late Quaternary evolution of Reedy Glacier, Antarctica. *Quat. Sci. Rev.* 29, 1328–1341.
- Waddington, E.D., et al., 2005. Decoding the dipstick: thickness of Siple Dome, West Antarctica, at the last glacial maximum. *Geology* 33, 281–284.
- Weaver, A.J., Saenko, O.A., Clark, P.U., Mitrovica, J.X., 2003. Meltwater Pulse 1A from Antarctica as a trigger of the Bølling–Allerød warm interval. *Science* 299, 1709–1713.
- Wellner, J.S., Lowe, A.L., Shipp, S.S., Anderson, J.B., 2001. Distribution of glacial geomorphic features on the Antarctic continental shelf and correlation with substrate: implications for ice behavior. *J. Glaciol.* 47 (158), 397–411.